Multiscale characterization of Li-ion batteries through the combined use of atomic force microscopy and X-ray microscopy and considerations for a correlative analysis of the reviewed data

Danilo Dini,*[a] Flavio Cognigni,[b] Daniele Passeri,[b] Francesca Anna Scaramuzzo,[b] Mauro Pasquali,[b] Marco Rossi*[b]

[a]*Department of Chemistry, University of Rome LA SAPIENZA, 00185 Rome, Italy*

[b]*Department of Basic and Applied Sciences for Engineering (SBAI), University of Rome LA SAPIENZA, 00185 Rome, Italy*

* email: danilo.dini@uniroma1.it; marco.rossi@uniroma1.it

Abstract

The present review analyses the recent literature on the combined use of X-ray microscopy (XRM) and atomic force microscopy (AFM) for the multiscale characterization of Li^+ (or Li) batteries (LiBs) with the aim of developing guidelines for their correlative analysis. The usefulness of XRM resides in the capability of affording non invasively *in situ* images of the inner parts of a LiB (an encapsulated device) with spatial resolution of dozens of nm during LiB operation. XRM is non destructive and affords the early diagnosis of LiBs degradation causes when these manifest themselves as microdeformations. The multiscale characterization of LiBs also requires AFM for visualizing the morphological/physical alterations of LiB components (anodes, cathodes, electrolyte) at the sub-nanometer level. Different to XRM, AFM necessitates of a modification of LiB working configuration since AFM uses a contacting probe whereas XRM exploits radiation-matter interactions and does not require the dissection of a LiB. A description of the working principles of the two techniques is provided to evidence which technical aspects have to be considered for achieving a meaningful correlative analysis of LiBs. In delineating new perspectives for the analysis of LiBs we will consider additional complementary techniques. Among various AFM-based techniques particular emphasis is given to electrochemical AFM (EC-AFM).

Introduction

LiBs are presently very diffused in the market especially as energy suppliers for consumers electronics and their commercialization is expected to grow in the immediate future considering the ulterior applicative ambits of electric vehicles [**1**] and energy storage systems.[**2**] LiBs then represent a very mature technology with solid perspectives of a further (not to say unavoidable) expansion in the next few years.[**3,4**] Given the widespread and extended use of LiBs at the global level the generic issues LiBs research poses are the quest of increased efficaciousness and durability,[**5**] the feasibility of LiBs recyclability/re-use (in economic and sustainability terms),[**6-9**] the diminution of costs,[**10**] the sustainability of large-scale production [**11,12**] and safety.[**13,14**] LiBs are characterized by having high energy densities and efficiencies, lack of memory effects, long life cycle and high-power densities.[**15**] This combination of properties allows LiBs to be smaller and lighter with respect to other rechargeable batteries, rendering LiBs suitable as a well-established solution for a wide range of applications like electronics, electric vehicles and mobile electronics among others [**16,17**]. In the coming years, the characteristics of LiBs are expected to be improved for the execution of better performances and for a major reliability when operating under extreme conditions of temperature, pressure, and rate over long lifetimes.[**18**] In this highly competitive research ambit LiBs aspects with dimensionality ranging from macro- to nano-scale such as assembly, porosity, tortuosity, solid-electrolyte interphase (SEI) growth and dendrites formation need to be studied more comprehensively and, more importantly, correlated.[**19**] All these parameters and phenomena should be adequately analysed and associated with the other features that overall dictate battery's reliability and long-term safety.[**20**] Moreover, macro-, micro- and nano-structural and electrochemical changes of LiBs should be studied before, during and after aging cycles in order to understand the reaction mechanisms underlying the various physical and chemical processes that control LiBs operation.[**21**]

In the following a review of the recent literature on the use of atomic force microscopy/microscope (AFM) and X-ray microscopy/microscope (XRM) for the multiscale characterization of LiBs will be presented. An introductory description of these techniques is also given. A conclusive section on the correlative analysis based on the results achieved with the various microscopy techniques here reported will be attempted.

Multiscale characterization of LiBs

1. LiBs analysis with AFM

1.1 Introduction to AFM

Different to microscopy techniques, where the image of the sample is obtained from the interaction between an incident electromagnetic beam with the matter, in scanning probe microscopy (SPM) a sharp tip is brought into close proximity with the surface of the sample.

The tip is then used to scan the surface and a physical parameter reflecting the tip-sample interaction is monitored. The magnitude of this parameter depends on the actual tip-sample separation distance and its variation on the surface is used to reconstruct the sample morphology. The actual physical parameter which is used identifies the different SPM techniques. In scanning tunneling microscopy (STM), a static voltage is applied between the conductive tip and the conductive sample while the parameter monitored during the surface scan is the tunneling current [**22**]. The most widespread SPM technique is AFM [**23**], in which short range repulsive (coulombic) or attractive (van der Waals) tip-sample interaction forces are monitored. Most commonly, the sample surface is reconstructed by monitoring the deflection of a microfabricated cantilever, at the end of which the tip is located. A laser beam is focused on the back of the cantilever in correspondence of the point of anchoring of the tip. The laser beam is than reflected and its displacement (coherent with the tip-cantilever movements) is recorded by a position-sensing four-segment photodetector. Different operation modes have been developed: i) in contact mode the tip is in contact with the sample surface during the whole scan experiencing coulombic repulsive force; ii) in semicontact mode the cantilever oscillates and the tip is in contact with the sample surface for a fraction of the oscillation period; iii) in non contact mode the tip never touches the surface interacting with it via van der Walls forces. As a result, in AFM the sample surface can be routinely reconstructed with nanometer lateral resolution and sub-nanometer vertical resolution. This allows also the visualization of crystalline lattices with atomic resolution.

1.2 Morphological characterization of LiBs components

The different modalities allow AFM to image a broad range of typologies of samples, obviously including materials for LiB which have been characterized both in air, *in situ* (literally "on-site"), and *in operando* (i.e. during operation), in particular in the so-called electrochemical AFM (EC-AFM) as discussed in the next section. For example, topographical imaging allowed to reveal nanoscale irreversible changes in the surface of $LiMn_2O_4$ cathode films after different charge/discharge cycles. These observations could be related to the ageing of the material [**24**]. Topographical analysis has been used to investigate the effect of repeated charge/discharge cycles on $LiCoO_2$ cathode films. Such a study revealed progressive surface modifications that could be quantified in terms of grain size and surface roughness [**25**]. Moreover, by varying the intensity of the tip-sample interaction, the AFM tip can be used to modify the sample surface and to monitor the effect of such nanomanipulation by the subsequent imaging of the area. As an example, the morphological analysis has been used to measure the thickness of the SEI formed on highly oriented pyrolytic graphite (HOPG) electrode through the scanning of the surface in AFM contact mode. This procedure allows the scratching of the SEI layer and, consequently, creates a step with the uncovering of the underlying HOPG electrode [**26**].
In AFM the nanometer sized tip can be located with nanometer accuracy also in the lateral position with respect to sample orientation. Such a feature allows the detection of ultralow interaction forces with the sample surface. Moreover, AFM constitutes a versatile platform for the development of different techniques that characterize simultaneously physical/chemical properties (e.g. mechanical, electric and magnetic properties among others), and afford the morphological reconstruction of the sample. This adaptive aspect of

AFM is particularly relevant since it allows the highly resolved mapping of a given property. Some of these methodologies have been employed, also in a synergistic way, in the study of LiBs materials. Such studies aimed at correlating the nanometer scale physical properties with the macroscopic ones and with LiBs performances. Different AFM-based techniques have been also used to combine morphological, structural, and mechanical properties with local electric properties like conductivity, surface potential, or work function. As an example, Yang *et al.* [**27**] analyzed the dependence of morphological, mechanical, and electric properties of lithium-rich thin films for cathode materials upon cyclic exchange of Li-ion. Also, Wu *et al.* [**25**] combined the analysis of morphology, mechanical properties with the analysis of $LiCoO_2$ surface potential. In particular, the variation of morphological, mechanical and surface potential properties of $LiCoO_2$ films during charge/discharge cycles was related with the macroscopic parameter of electrical capacity.

1.3 Evaluation of mechanical properties

The type of variations of the mechanical properties of LiBs electrodes during charge/discharge cycles affect the performances of LiBs and determine the ageing of the electrode materials. While standard nanoindentation allows the characterization of elastic modulus with micron-scale lateral resolution, AFM-based methods enable the measurement of the same parameter with nanometer lateral resolution. Moreoveor, AFM maps the elastic module on the surface affording simultaneously the topographical reconstruction of the surface itself. When the AFM tip is used as an indenter, force spectroscopy can be performed: this technique enables the simultaneous evaluation of indentation modulus and the hardness of relatively compliant materials [**28**]. In order to overcome the calibration issues due to the uncertainty in the shape and dimension of the tip [**29**], colloidal probes can be employed. These probes are obtained by gluing spherical microparticles with known radius at the end of tip-free AFM cantilevers. Nguyen *et al*. [**30**] used AFM-based nanoindentation with colloidal probes employing Au spherical particles with radius of 7-9 μm. This expedient afforded the characterization of the elastic modulus of different polymer binders – e.g. polyacrylic acid (PAA), polyacrylonitrile (PAN), polyvinyl alcohol (PVA), carboxymethyl cellulose (CMC), and polyvinylidene fluoride (PVDF) – in use in LiBs. Despite the improved accuracy in the measurement of elastic modulus, AFM nanoindentation with colloidal probes does not afford simultaneously a high resolution mapping of mechanical properties and surface morphological characterization. To circumvent the limitations of the use of a colloidal tip the amplitude modulation-frequency modulation (AM-FM) technique is adopted. AM-FM is a dual frequency intermittent contact technique in which the first resonant mode of the cantilever is excited to acquire the morphology in tapping mode while the second resonant mode is used to map the local tip-sample contact stiffness. With AF-FM, after proper calibration of the tip, a highly resolved map of the indentation modulus can be obtained [**31**]. AM-FM in air and at room conditions has been used to study the evolution of nanoscale mechanical properties of $LiMn_2O_4$ cathode films. The study revealed the loss of homogeneity and the overall diminution of the elastic modulus after different cycles. This was related to the concomitant loss of capacity and was ascribed to decrease in the Li concentration

[24]. Analogous results were obtained on Li-rich and $LiCoO_2$ film cathodes, where cycling resulted in the reduction of the elastic modulus [25,27]. Zeng *et al*. [32] monitored the changes in the morphology and in the stiffness of nanoparticles of Li-rich layered oxide cathode materials as a function of the applied bias voltage, which led to the fracture of the nanoparticle. Also, AM-FM was successfully used to study diamond-like carbon (DLC) - ZnS double layer thin-film anodes [33]. It was observed an improved cycling stability with respect to that of pure ZnS thin-film anode.

PeakForce Tapping™ is another intermittent contact AFM technique where the surface is scanned by exciting the cantilever at low frequency, well below its first resonance, while the maximum cantilever deflection is maintained constant. The latter condition corresponds to the maximum force exerted on the surface (this is also indicated as peak force). Based on this approach , PeakForce Quantitative Nanomechanical Mapping (PF-QNM) allows the acquisition and the real time analysis of force-distance curves. PF-QNM enables the simultaneous quantitative mapping of topography, local values of the elastic modulus, tip-sample adhesion force, and the energy dissipated during each interaction cycle [34]. Being effective on relatively compliant materials, Huang *et al*. [26] used PF-QNM to investigate the morphological and mechanical properties of SEI formed on HOPG electrodes in various electrolytes, while Zhang *et al*. [35] used PF-QNM to investigate SEI formed on graphite anodes in presence of vinylene carbonate (VC) and fluoroethylene carbonate (FEC) used as additives. In the latter case it was observed the formation of thinner, stiffer, and more stable SEI layers with the consequent improvement of batteries performances. Also, PF-QNM has been used to assess the stability upon cycling of Li-S cathodes in presence of PVDF and CMC used as binders [36].

The so-called Nanoswing is an AFM based nanomechanical characterization technique which is based on the simultaneous imaging of the topography and acquisition and analysis of the torsional oscillation signal of the cantilever.[37,38] Nanoswing has been employed in the investigation of $LiMn_2O_4$ and $LiMnPO_4$ in form of nancrystalline powders to assess the differences in their mechanical and adhesive properties. In particular, Nanoswing revealed the higher chemical and structural stability of $LiMnPO_4$ with respect to $LiMn_2O_4$. Therefore, $LiMnPO_4$ is expected to represent a more attractive cathode material for long life LiBs [39].

In the conclusion of this session, it has been amply demonstrated that several AFM-based techniques can be successfully used for the accurate characterization of the mechanical properties of LiB materials with nanometer lateral resolution. This aspect is fundamental for the development of more stable devices during charge/discharge cycles. Nevertheless, the selection of a specific technique must take into due consideration the range of elastic modulus of the materials to be characterized. Indeed, the application of indentation based techniques, like AFM nanoindentation or PF-QNM, is generally limited to relatively soft materials, while contact resonance frequencies based techniques, like AM-FM, can be used on a broader range of materials. A second issue is represented by the depth down to which a material has to be analyzed. This is a particularly crucial aspect for layered materials. Such a capability varies dramatically for the various AFM-based techniques [40].

1.4 Evaluation of electric properties

1.4.1 Conductivity

The possibility of realizing conductive AFM tips, e.g. through the deposition of a metallic coating, allows the application of a voltage between the tip and the sample. As a response to the electrical potential stimulus the system tip-sample will be traversed by a measurable electrical current the extent of which will depend on the local conductivity properties of the sample as well as on the tip-sample spacing. In this context AFM can afford the mapping of the conductivity variations on sample surface through the employment of the conductive AFM (C-AFM) version. Yang *et al.* [**24**] used C-AFM to investigate the reduction of conductivity due to the nonconductive SEI layer on $LiMn_2O_4$ cathode films. C-AFM allowed the mapping of the nanoscale conductivity of lithium-rich thin film cathodes and determined a diminution in conductivity for these cathodes with charge/discharge cycles. At the macroscopic level this finding was correlated to the observed decay of capacity [**27**]. Moreover, the variations of nanoscale conductivity have been also associated to reaction, diffusion, and accumulation of Li^+ ions in the cathode materials [**32**]. Nagpure *et al.* [**41**] reported a decrease in local conductivity for $LiFePO_4$ cathodes and ascribed this observation to both physical and chemical changes at the surface. These changes mostly consisted in the coarsening of the nanoparticles constituting the film and the formation of nanocrystalline deposits on the surface. Upon cyclic variation of the bias voltage between tip and sample, the current-voltage curves showed hysteresis. The latter phenomenon in Li-rich cathodic materials has been related to local concentration and mobility of Li in the probed volume of material [**42**]. Due to the simultaneous morphological and electric mapping at the high spatial resolution provided by C-AFM, Chen *et al.* [**43**] investigated the conductivity and the Li de-intercalation on different facets of $LiCoO_2$ crystals. The work showed two different evolutions of conductivity and assessed the capability of the different crystal facets to reduce the internal resistance of batteries.

PeakForce TUNA™ mode is an intermittent contact C-AFM technique which was combined with elastic modulus measurements. Such an experimental set-up was employed for the study of the stability of Li-S cathodes prepared with PVDF and CMC as binders. The analysis evidenced the better performances of batteries prepared with PVDF binder with respect to CMC in terms of lower reduction of conductivity upon cycling [**36**].

1.4.2 Surface potential

Among the different electric properties that can be investigated at the nanometer scale with AFM based techniques, surface potential and work function are undoubtedly the most important ones for the characterization of LiB materials. In Kelvin probe force microscopy (KPFM), an oscillating voltage is applied between the conductive AFM tip and the sample resulting in a mechanical oscillation of the cantilever which depends on the static tip-sample bias. The cantilever oscillation can be nullified by varying the dc bias thus determining the local value of surface potential. The latter parameter can be eventually used

to evaluate and map the work function of the sample [**44**]. KPFM has been used to map the surface potential distribution on different cathode materials, e.g., $LiCoO_2$ [**25**] or $LiFePO_4$ [**45**], in order to assess its variation after charge/discharge cycles. Chen *et al*. [**43**] used KPFM to measure the work function on different facets of $LiCoO_2$ crystals, which corresponded to two preferred crystallographic orientations. The observed differences were attributed to the mechanism of formation of the cathode/electrolyte interphase. KPFM was recently employed also for characterizing the variation of surface potential between different polymer electrolytes, i.e., polyethylene oxide and poly[bis-2-(2-methoxyethoxy)-ethoxyphosphazene], and different ionic-electronic ceramic particles [**46**]. Moreover, KPFM has been used to characterize the cross section of solid state LiB and to image the internal distribution of electric potential [**47**]. The study evidenced the depletion of Li ions with high lateral resolution and, at the same time, highlighted the importance of the evaluation of structural parameters at both micrometer and nanometer scale in composites electrodes.

2. Electrochemical Atomic Force Microscopy (EC-AFM) for LiBs analysis

2.1 Generalities of EC-AFM

The field of EC-AFM involves all those cases in which an atomic force microscope is employed for the topographic investigation of the surface of a constituent of an electrochemical cell.[**48-54**] EC-AFM represents a SPM technique [**55,56**] since it is based on the combination of an AFM and an electrochemical function generator as basic units of the experimental set-up (Figure 1a).[**48,54**] In the ambit of EC-AFM the electrochemical cell is opportunely assembled around the scanning probe of the AFM head (Figure 1b) in order to accomplish in an optimized way the desired electrochemical reaction while probe scans the electrode surface in a close contact mode.[**54**] The immediately recognized merit of EC-AFM consists in the possibility of realizing *in situ* the high-resolution topographic investigation of the electrode surface when this is immersed in an electrolytic solution while the electrode is under galvanostatic, potentiostatic or potentiodynamic control.[**56**] Such a possibility allows operators to correlate the electrode activity with surface topography [**55**] provided that the scanning probe head with its volume does not interfere critically with the transport dynamics of the electrochemical reaction.[**54**] In fact, one of the major difficulties EC-AFM experimentalists have to deal with is the attenuation of the undesired systematic effect of AFM head tampering: this consists in the impediment of the flow of the electrochemical/charge compensating reactants towards or from the electrode surface due to the unavoidable presence of the AFM head holding the scanning probe.

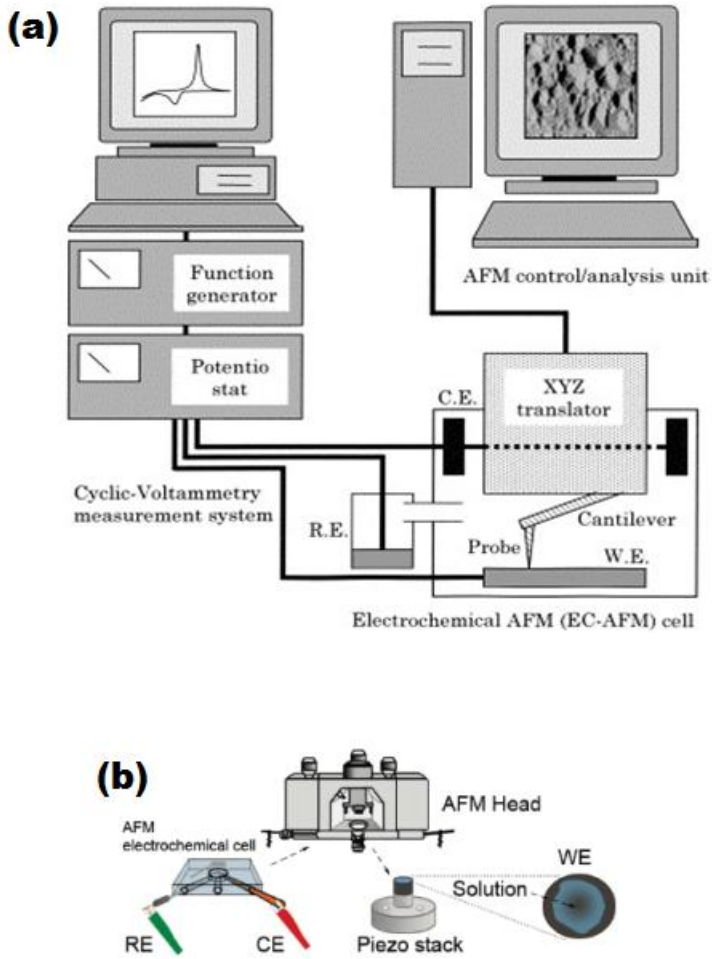

Figure 1. (a): Scheme of the experimental set-up adopted for the realization of EC-AFM experiments. From ref. **48**. (b): Sketch of an example of AFM head combined with a three-electrode electrochemical cell. From ref. **54**.

EC-AFM has been succesfully employed in the study of LiBs [**57**] for the *in situ* topographical characterization of a battery electrode in contact with a liquid electrolyte.[**58-62**] Incidentally: a major future challenge EC-AFM will have to face is its employment in the *in situ* study of LiBs with all solid-state configuration.[**63,64**] Such a cell configuration is characterized by having hardly accessibile interfaces for which instrumental adaptations will be necessary. The extension of the use of EC-AFM on all-solid-state systems serves to complement the information given by the synchrotron radiation-based techniques[**65-74**] the latter being nowadays the most sophisticated approach apt to investigate all solid-state LiBs.

Synchrotron-based techniques provide information on local structure, chemical and phase composition in form of map images thanks to the high brilliance of the X-ray radiation (*vide infra*) [**65-74**]. Besides the investigation of the properties already discussed in the previous section, AFM has proven to be a powerful tool to get an insight into the working mechanism of LiBs monitoring, for example, the electrodes consumption and the development of SEI (*vide infra*). This is possible by means of *in situ* AFM and EC-AFM, which operate in fluid electrolyte using the scanned surface as electrode. The cell is completed by inserting a suitable counter electrode (Figure 1). Basically, in this way a full electrochemical cell is obtained within the AFM sample holder and the tip scans the electrode surface *in operando* conditions. This affords the monitoring of what is actually occurring at the surface during charge/discharge cycles. In order to get information on LiBs *in operando*, it is necessary to guarantee inert atmosphere for the high reactivity of LiBs components in ambient conditions (*vide infra*). This can be circumvented by putting the AFM set-up in a glove box filled with Ar or N_2. In the following sections we will describe the main results achieved by means of *in situ* EC-AFM when anodes and cathodes of LiBs were analyzed.

2.2 EC-AFM for the analysis of LiBs anodes

In the ambit of LiBs research *in situ* EC-AFM studies have been prevalently dedicated to the analysis of the process of SEI formation onto graphite,[**35,75**] lithium [**76-78**], silicon,[**79-83**] graphene [**84**] and HOPG anodes.[**26,85,86**] SEI is a passivating film which forms at the interface between anode and electrolyte. As a matter of fact, SEI plays a crucial role for safety and long lasting of batteries since it causes an irreversible loss of capacity offset by a general improvement of electrode stability over the cycles. Being nowadays graphite the benchmark for anodes in commercially available LiBs, the vast majority of studies has been performed on HOPG surfaces as scanned sample. The observation of morphological changes in HOPG during cyclic voltammetry at slow scan rate highlighted the formation of hill- and blister-like structures at potential values that depended on the composition of the electrolyte. The origin of these protuberations was attributed to the intercalation and decomposition of solvated lithium ions. The formation of SEI takes place in different steps as a function of the negative electrode potential [**87**]. As expected, the main morphology changes of the electrode were observed at the beginning of each experiment with verification of the partial dissolution/redeposition of the surface layer up to the five first cycles thus confirming that SEI formation is overall irreversible [**88**].

In addition to lithium-based reactions, at very negative potential solvent decomposition can also occur. This fact highlights the importance of the chemical nature of the electrolyte for the capacity of the battery. The reduction of solvent molecules facilitates the electrode consumption. This can be a consequence of the formation of gaseous species or in case of the presence of fissures in the pristine surface. [**89,90**] Moreover, the solvent can undergo co-intercalation as part of the solvation shell surrounding lithium cations. AFM images of HOPG basal plane surface before and after the first voltammetry cycle showed that solvent co-intercalation takes place more extensively in case of the mixture ethylene carbonate (EC)/diethyl carbonate

(DEC) in comparison to EC/dimethyl carbonate (DMC) or pure EC. These observations suggested that the nature of the linear alkyl chains played a role in co-intercalation phenomena [**91**].

Besides the analysis of the morphological changes, *in situ* EC-AFM was exploited to study the behavior of different HOPG planes, thus contributing in the elucidation of the mechanism of SEI formation[**92**]. When coupled with cyclic voltammetry continuous *in situ* AFM imaging evidences that during the first cycle the thickness of the edge plane increases faster than that of the basal plane. On going from the first to the successive cycles the increase of the thickness of the basal plane becomes larger than that of the edge plane. Even though the resulting film is not homogeneous, this observation suggested that the edge plane is covered by a passivating film in the first cycle more effectively than the basal plane. It was concluded that the edge plane participates more actively to the decomposition reaction of the electrolyte.

More recently, the combination of EC-AFM with different techniques, either home-made or home-assembled, opened new perspectives in evaluating simultaneously the different properties of SEI. As an example, EC-AFM with multiple operation modes allowed to quantitatively evaluate thickness and mechanical properties of SEI, confirming the polymeric nature of the interphase.[**93**]

In operando EC-AFM demonstrated that SEI is much thicker and softer at edge sites with respect to the one formed on the basal plane after the correlation of the modulus mapping with the morphology imaging of SEI during formation.[**35**] By adding vinylene carbonate (VC) and fluoroethylene carbonate (FEC) an enhanced SEI layer (thinner and stronger) was formed. This type of SEI improved the overall battery performance when the layer developed at both edge and basal areas of the graphite. Moreover, in the same study the influence of the starting material used as electrode has been demonstrated showing that the model HOPG substrate show significantly different behavior with respect to the graphite particles used for anodic industrial production. The effect of the starting material properties on the SEI formation has been confirmed by Luchkin and co-workers,[**94**] who used *in situ* AFM to observe SEI nucleation and growth on various substrates [HOPG, MesoCarbon MicroBeads (MCMB) graphite, non-graphitizable amorphous carbon (hard carbon)]. Under the same experimental conditions, each type of anode showed a characteristic potential value for SEI formation (about 0.8 V for HOPG edge sites, 0.5 V for HOPG basal plane sites, 0.8-0.9 V for MCMB graphite, ca. 0.4 V with the preliminary weakly bound deposit at about 1 V for hard carbon). The SEI layers on MCMB and hard carbon were thicker and stronger than the SEI on HOPG being the SEI rich in polymer products on the basal plane of HOPG. On the other hand, the SEI formed on a highly porous substrate is scarcely prone to delamination given its tendency to penetrate into the superficial porous.

The combination of EC-AFM and SECM allows the attainment of both topographic and surface electrochemical properties for SEI. Ventosa and co-workers used a glassy carbon electrode as model system for a graphite electrode LiB [**95**]. They monitored the formation of the SEI by means of *in situ* AFM during the first electrochemical reduction. In a subsequent step, AFM was employed in the high-force contact mode to remove a defined area of 50 μm x 50 μm of SEI film. Besides the analysis of the scratched area, the sample was studied with SECM in the feedback mode. The latter allowed the monitoring of the changes in the conductive and redox properties as a function of the presence/partial removal of the SEI. It is known

that SEI properties can be influenced by the presence of additives in the electrolyte [**96**]: EC-AFM and multiple *in situ* AFM showed that SEI top layer on HOPG formed in EC consisted mainly of alkyl carbonate-based scattered islands. In the presence of fluoroethylene carbonate (FEC) SEI top layer is LiF-based and results thicker and more densely packed in comparison to the one formed with EC. The SEI formed in FEC environment enhanced the stability and cyclability of the anode. For the development of LiBs nowadays aqueous electrolytes are also considered although relatively few studies have been conducted on these systems. In a recently published paper, [**76**] *in situ* AFM images showed the morphological evolution of SEI in the presence of 21 M lithium bis(trifluoromethane sulfonyl) imide aqueous electrolyte. In addition to this, the combined use of EC-AFM and *ex situ* (i.e., "off-site") X-ray photoelectron spectroscopy revealed that the afore-mentioned aqueous electrolyte-based SEI is inhomogeneous, being the inner layer mainly composed of Li_2CO_3 and outer layer mainly composed of LiF. This SEI, with a thickness of 4–6 nm, showed a high Young's modulus part of about 30 ± 10 GPa, and a low Young's modulus part of about 1-2 GPa. The results indicated that SEI was made of both inorganic species (rigid) and organic species (more elastic).

By means of EC-AFM and EC-STM coupled with cyclic voltammetry it has been also demonstrated that the early stages of anion intercalation are highly affected by a number of factors like surface faceting, step erosion, terrace damages, and nanoprotrusions.[**97,98**] From these studied it emerged that AFM resulted particularly sensitive in detecting the very early stage of intercalation. Once SEI is formed, the subsequent process of intercalation/deintercalation of lithium cations within the graphite layers is basically reversible. On the other hand, electrode surface is inevitably stressed and stretched especially on the edge planes of the expansion. The knowledge of dimensional changes during intercalation of lithium cations is crucial for the full understanding of the mechanism of anodic degradation. *In situ* EC-AFM can actually monitor the changes in the morphology of the anode over the charge/discharge cycles, i.e. during subsequent intercalation/deintercalation of lithium cations within the graphite layers. It is worth noting that the passivating film formed in the first cycles is not totally homogeneous and compact. This is due to the presence of lithium salts. Probing the surface at sub-nanometric scale with an AFM can be rewarding since it monitors even a very slight, irreversible morphological change of graphite electrodes in liquid electrolyte as a consequence of the continuous reactions of solutions species with lithiated graphite[**99**]. Such reactions lead to a fade of battery capacity over the time. EC-AFM has been successfully exploited to monitor the variation in graphene interlayer distance of a HOPG electrode during lithium intercalation and de-intercalation[**100**]. The height of a HOPG step has been obtained from AFM images by calculating the difference between the mean values of the heights measured on different locations on the steps for different images at different potential. After the starting irreversible increase of layer spacing, over the cycles the reversible swelling/shrinking of the electrode has been measured to be of about 17%.

2.3 EC-AFM for the analysis of LiBs cathodes

Cathode materials for LiBs are usually metal oxides able to intercalate/deintercalated lithium ions within their crystalline lattice without any significant disruption. In comparison to anodes, cathodes have been less deeply studied via EC-AFM. As far as the cathodic materials of LiBs are concerned, the employment of *in situ* EC-AFM has regarded mostly the topographic and mechanism investigation of the processes consisting in the solid state transformations of $LiMn_2O_4$, [**50,101**] $LiFePO_4$, [**102,103**] Li_2S[**104,105**] and $LiNi_xMn_yCo_{1-x-y}O_2$ (NMC)[**106**] during lithiation/delithiation cycles. A typical information of EC-AFM is represented by the visualization of the Li deposit occurring on a graphite surface during galvanostatic charging (Figure 2) [**75**] or the formation of a SEI layer during cyclic operation of a HOPG anode (Figures 3 and 4) [**35,76**]. Another example of the use of EC-AFM is represented by the visualization of the morphological changes occurring in $LiFePO_4$ during charge/discharge cycles (Figure 5).[**102**] Nowadays most commercial LiBs have a $LiCoO_2$ cathode. In 2007, Shao-Horn and co-workers [**107**] reported a detailed study on surface and dimensional changes of individual Li_xCoO_2 crystals during lithium de-intercalation by mean of *in situ* and *ex situ* EC-AFM. They first noted that Li_2CO_3 impurities – already known from the literature - are actually present not as a uniform layer but as discrete particles that tend to dissolve gradually into the $LiPF_6$-containing electrolyte. During deintercalation, upon observation along the c_{hex} axis, no surface instability or structural instability could be detected. Moreover, the general morphology of Li_xCoO_2 crystals remained unvaried. Continuous AFM imaging revealed an excellent dimensional stability, with a change in the step height of about +1.7% at the end of charge. Other cathodic materials studied by EC-AFM are vanadium oxides [**108**] that are known for presenting different oxidation states for the vanadium centers. As a consequence of that LiBs possessing cathodes of vanadium oxides can present high capacity. By means of slow-scan cyclic voltammetry it has been demonstrated that it is possible to obtain faster kinetics of intercalation for lithium ions into the layered V_2O_5 cathodes when the supporting electrolyte is $LiClO_4$ in comparison to $LiPF_6$. Electrolyte containing $LiPF_6$, in turn, seem to induce capacity fading over cycles. This empirical evidence has been explained at a microscopic level by means of *in situ* AFM: the nano-size particles originating from $LiPF_6$ solutions deposit onto the boundaries of the V_2O_5 grains thus slowing down the insertion of lithium ions into the layered matrix. Such a deposition induced a detrimental effect on the overall electrochemical performance. On the other hand, the same study stated that no substantial morphological changes at the cathode could be detected in presence of ClO_4^- ions. Concerning the intercalation/deintercalation mechanism and subsequent electrode changes, EC-AFM could monitor the lateral extension and contraction of the vanadium oxide nanograins as well as the flattening of the oxide film surface [**109**]. Upon intercalation, the oxide undergoes a transition from α to δ phase, with a consequent lateral extension of up to 15%. During deintercalation a lateral contraction of the oxide grains is observed. However, the residual subsisting lateral extension of the grains indicates that the nanostructural surface modifications are not fully reversible upon cycling. Such aging phenomenon, together with the modification of oxide grains surface upon creation of new ridges and new surface steps, determines the consumption of the electrode material over cycling. Very similar to what reported for vanadium oxide cathode, the $LiFePO_4$

film electrode obtained via radio frequency magnetron sputtering was investigated in aqueous environment by *in operando* EC-AFM with the monitoring of the changes in grain area [**102**]. The size of the grains decreased and increased respectively during charge and discharge, but such variations did not result totally reversible.

Finally, EC-AFM was used by different research groups to characterize $LiMn_2O_4$ [**50,101**]. Detailed structural and electrochemical studies of $LiMn_2O_4$ cathode in $LiPF_6$ electrolyte using *in situ* EC-AFM and lateral force microscopy have been conducted to elucidate the surface reaction occurring during charge/discharge cycles. The surface topological changes observed at the open-circuit voltage suggested that the cathode material reacts as soon as it comes in contact with the electrolyte $LiPF_6$ when is dissolved in a mixture of EC, DMC and DEC. Furthermore, when surface dynamics was monitored under various charge/discharge conditions it was found that during cycling a variety of processes occurred: these involved different dissolution/precipitation reactions of lithium and manganese compounds containing phosphorus and fluorine [**50**]. In order to minimize the impact of such a complex ensemble of reactions, it was suggested to modify the cathode by mean of a polymeric coating of poly(diallyldimethylammonium chloride) (PDDA) [**110**]. As expected, this cathode material exhibited enhanced stability during charge/discharge cycles as well as less capacity fading. In this context, EC-AFM proved again to be extremely useful since it showed only minor changes in surface topography of the coated electrode with respect to the ones observed for the pristine material. More recently, thanks to the development of an electrochemical high-speed AFM (EC-HS-AFM) it has been possible to monitor dynamic morphological changes in the $LiMn_2O_4$ nanoparticles during cyclic voltammetry measurements [**111**]. EC-HS-AFM represents an advanced tool with a sophisticated design which couples technologies capable to detect small cantilever deflection with a dual scanner capable of high-speed and wide-range imaging. In detail, the scanning of spinel nanostructured $LiMn_2O_4$ (with an average size of about 300 nm) evidenced a volume change rate of less than 10% during lithium cation intercalation/deintercalation. Moreover, EC-HS-AFM with a collection speed up to 600 times faster than conventional EC-AFM), revealed that some nanoparticles moved upward relative to the others when the potential was scanned in the positive verse. The opposite movement was observed with the nanoparticles moving downward back to their original state in the reverse scan with a maximum height of displacement of about 55 nm. This phenomenon was ascribed to the intrinsic instability of the nanoparticles and revealed possible interactions between the nanoparticles during the electrochemical reaction. A conventional EC-AFM apparatus would not detect such phenomena. Apart from the information provided for the particular case of $LiMn_2O_4$ cathodes in LiBs, EC-HS-AFM is undoubtedly a technique of more general interest for the monitoring of batteries *in operando* and for analyzing processes of fast charging or SEI formation at interface.

Despite the advancements some critical aspects on the general use of EC-AFM still persist. In fact, as every AFM-based technique, EC-AFM suffers of the fact that is informative of the changes occurring at the surface/interfacial level of an electrodic sample but does not give any direct insight on the eventual modifications occurring at the bulk level of the electrodic material during a redox process.[**112**] This might

represent a limit in those cases where electrodes undergo solid-state electrochemical reactions and there is the involvement of electrode bulk at high levels of intercalation (*vide supra*).[**113,114**] Moreover, due to the high spatial resolution of the AFM technique the area spanned by AFM is usually confined within few dozens of square micron.[**112**] Another limitation of EC-AFM is represented by the lack of chemical information that can be simultaneously combined with the morphological, mechanical and electrochemical information.[**112**] In the past, EC-AFM presented the problem of how to handle and transfer air-/water-sensitive samples or cell components/materials.[**112**] Fortunately, newer versions of EC-AFM now include the option of gas-tight chambers that are capable of hosting the AFM head and the electrochemical cell in inert atmosphere [**115**]. Such instrumental solutions afford the necessary mechanical stability for recording non noisy signals from the EC-AFM inside the chamber and eliminate all limitations associated with the manipulation of reactive samples.

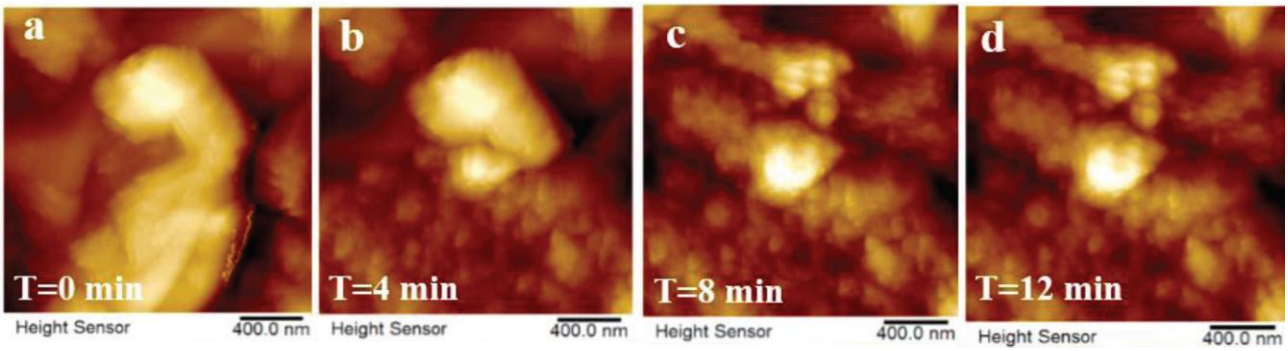

Figure 2. Image of the height on a graphite surface undergoing lithium plating at different times of galvanostatic deposition in EC/DMC mixture and $LiPF_6$ as supporting electrolyte. From ref. **75**.

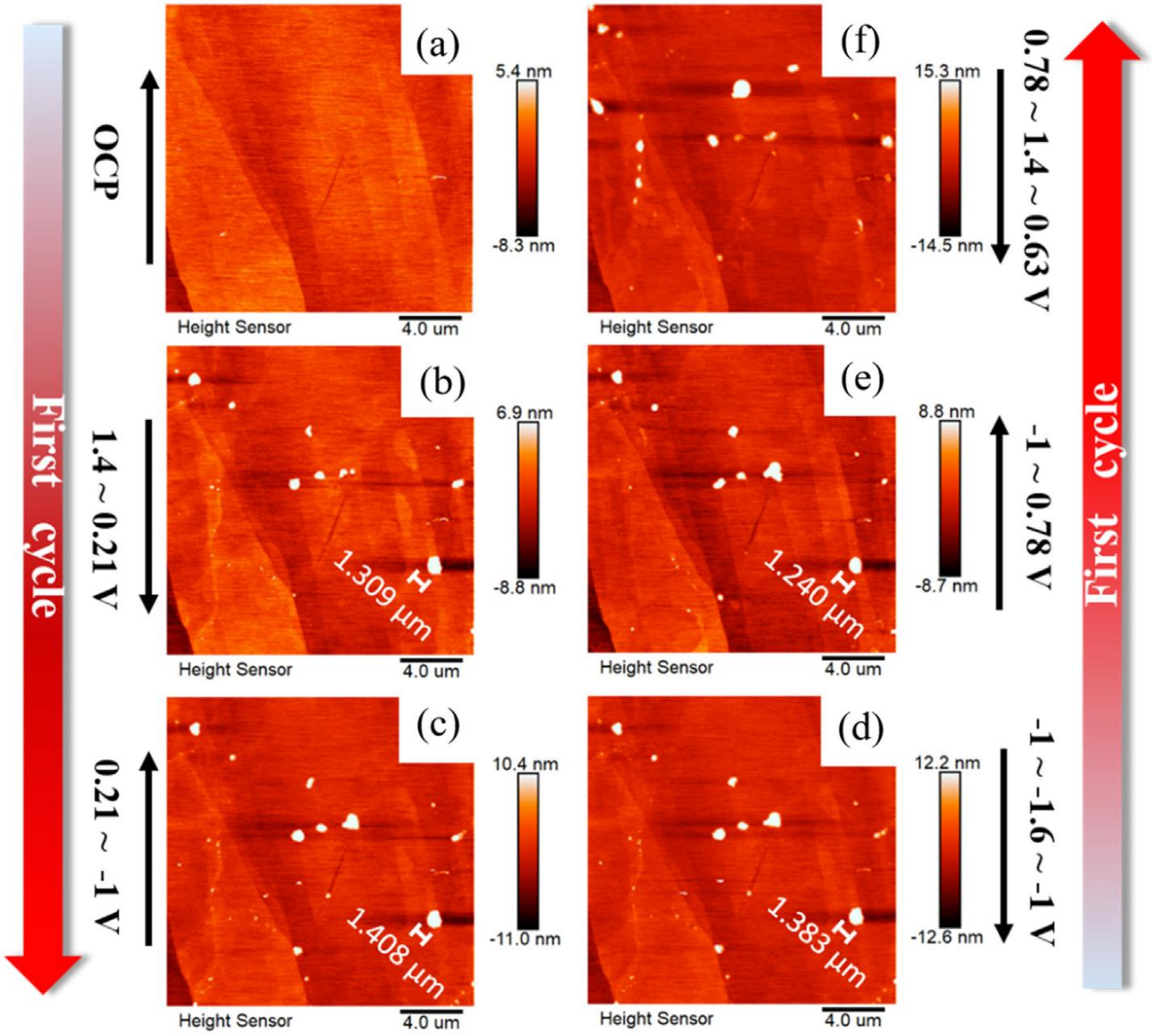

Figure 3. *In situ* AFM images showing the onset of SEI formation onto HOPG electrode. From ref. **76**.

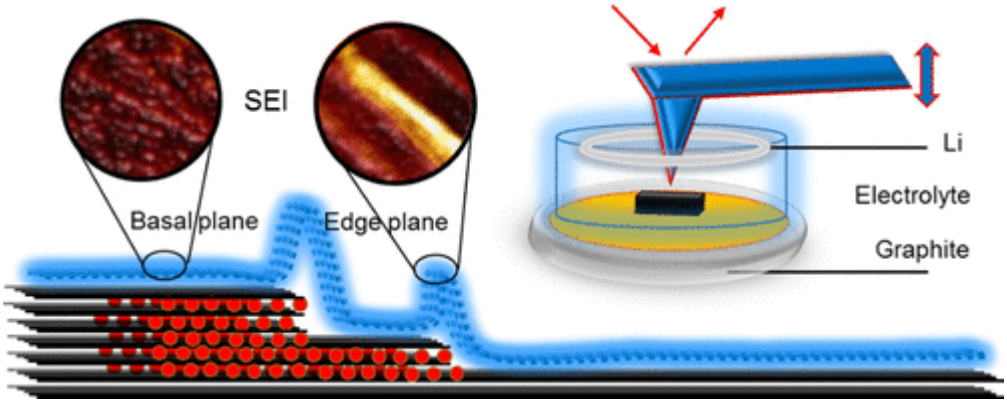

Figure 4. Representation of the SEI profile on the edge and basal planes of graphite substrate. In the inset the scheme of the EC-AFM employing a graphite substrate as working electrode and a ring-shaped counter electrode of Li is depicted. From ref. **35**.

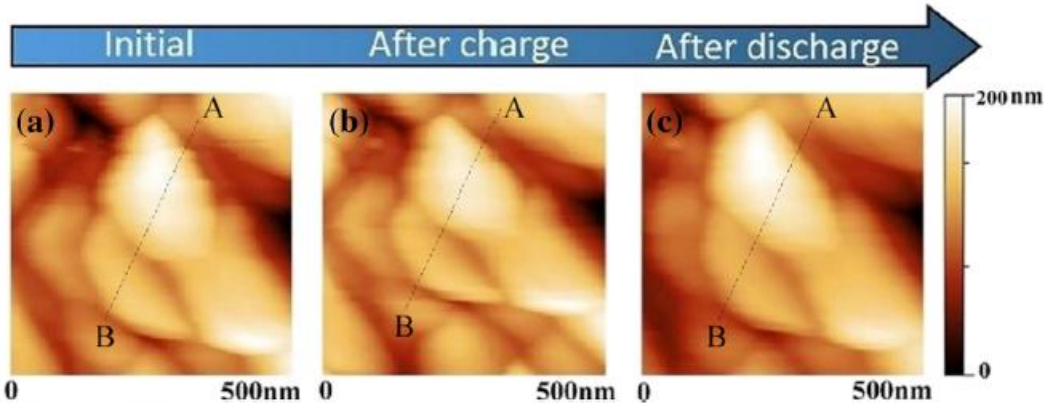

Figure 5. AFM images of $LiFePO_4$ cathode undergoing a change of grain shape and size during charge-discharge measurements conducted galvanostatically in aqueous electrolyte at 20 μA cm^{-2} of current density (from ref. **102**).

3. Use of XRM in LiBs research

3.1 Basic principles of XRM

X-ray microscopy (XRM) is a non-destructive characterization technique that can provide quantitative information on chemical/phase composition, and offers the possibility for a multiscale and multimodal 2D/3D investigation of the sample [**116**] employing an experimental set-up composed of three main elements: i) the source producing the X-ray beam; ii) the sample stage that ensures the mechanical stability of the sample and allows its rotation/orientation during analysis; iii) the detector [a charge-coupled device

(CCD) or a complementary metal-oxide semiconductor (CMOS)] which collects X-rays coming from the object [**117**]. When X-rays pass through a sample they undergo a partial absorption with the diminution of their intensity according to the Beer-Lambert law:

$$I(L) = I_0 e^{-\int_0^L \mu(x)dx} \qquad \{1\}$$

where $I(L)$ represents the transmitted X-ray beam intensity (in Watt), I_0 is the incident X-ray beam intensity (in Watt) and $\mu(x)$ (in m^{-1}) is the attenuation coefficient value at a certain position x (in m) within an heterogeneous material with length L (in m). Equation 1 reports an exponential decrease of X-ray beam intensity with the traversed distance when the phenomenon of the absorption of a quasi-monochromatic X-ray beam passing through a heterogeneous specimen has to be analysed (Figure 6).

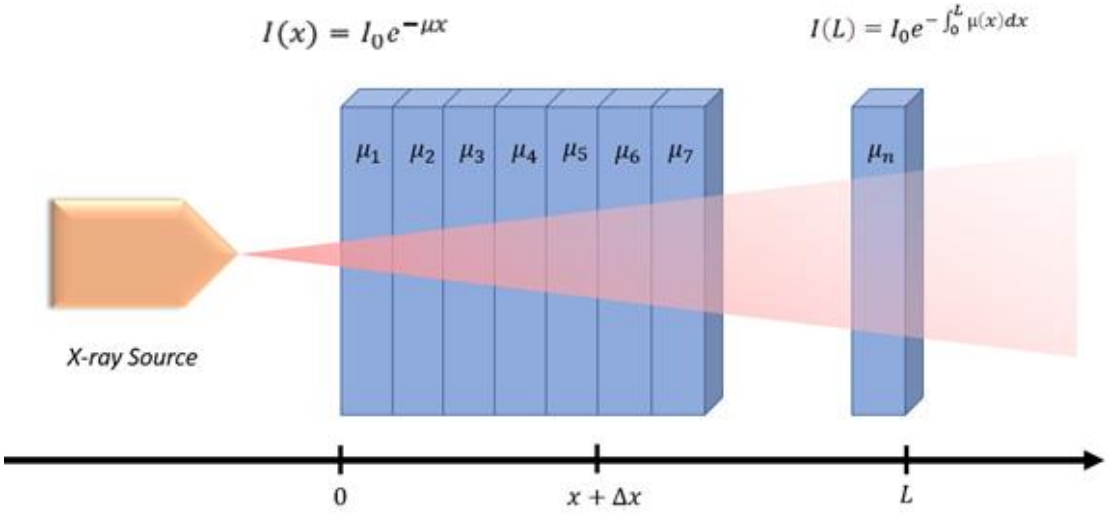

Figure 6. Attenuation of X-rays intensity in accordance to the exponential law of Beer-Lambert when the beam traverses an heterogeneous sample (with total thickness L) constituted by n adjacent layers of homogeneous material. X-rays attenuation within a homogenous layer is controlled by the attenuation coefficient m_i of the corresponding material and depends on layer thickness x_i (left equation). For an object composed of n different materials with attenuation coefficients $\mu_1, \mu_2, \mu_3, \ldots \mu_n$ the overall attenuation obeys the principle of additivity (right equation). From ref. **117**.

The transmitted X-rays reaching the detector are converted into visible light by a scintillator. The response of the scintillator is successively imaged and magnified by a camera. This allows the attainment of a single projection image of the sample [**118**]. The process is repeated iteratively upon change of specimen orientation with respect to the direction of beam incidence. A set of projections is acquired and then used to obtain a 3D reconstruction of the object when fed into a tomographic reconstruction algorithm. A detailed

description of reconstruction algorithms can be found in refs. **119,120**. The 2D/3D map refers to the imaginary part of the refractive index of the specimen, i.e. the parameter sensing the changes in X-rays amplitude when the beam passes through the sample. This technique is typically referred as absorption contrast tomography. However, the irradiation with X-rays can lead to the determination of other measurable quantities such as the real part of the complex refractive index of the materials, which is related with the change in wavelength of the X-ray along its path through the samples with consequent occurrence of a phase shift between X-rays. This phenomenon results in an interference pattern that is superimposed onto the attenuation-based image. Bright and dark fringes appear at the interface of two different materials. This procedure is known as phase contrast tomography, and it is particularly suitable for low density materials which show a weak absorption [**121**].

X-ray characterizations can be also run using synchrotron facilities [**65-74**]: synchrotron radiation offers high brilliance, excellent directionality and a high X-ray flux that enhance the contrast when low density materials are studied. Moreover, synchrotron radiation allows to achieve high temporal resolution for systems undergoing changes (*vide supra*). However, the access to synchrotron facilities is typically limited and costly. For these reasons, laboratory X-ray microscopes, that are relatively easier to use and less expensive, have faced a significant improvement in terms of spatial resolution, imaging speed and target radiation dose. X-ray microscopes generally rely on geometric magnification *M* that is determined by the position of the specimen with respect to the source and the detector. Magnification is given by:

$$M = \frac{a+b}{a} \qquad \{2\}$$

where *a* and *b* represent respectively the Source-Object Distance (SOD) and the Object-Image Distance (OID), the image being the detector. Geometric magnification can be combined with finer focusing optics that allow for a sub-micron resolution and nanoscale imaging. Several examples of laboratory X-ray microscopes are available on the market any of each offers special features and specific optimizations.

3.2 XRM for LiBs diagnostics

X-ray characterization techniques offer the unique capability to investigate LiBs several times in a non-destructive way, across multiple length-scales and under different conditions running *ex situ*, *in situ*, and *in operando* experiments in the so-called 4D characterization. As discussed in the following paragraph, *in situ*/*in operando* experiments are privileged for LiBs characterization since LiBs undergo many chemical reactions operating over time and, consequently, alter several features at different length-scales. To understand these mechanisms, different experimental setups and techniques have been developed for XRM such as *ex situ*, *in situ* and *in operando* [**122**]. The most common *in situ*/*in operando* X-ray characterization techniques are X-ray imaging techniques including Transmission and Scanning X-ray Microscopy (TXM and STXM) and X-ray Computed Tomography (XR-CT); X-ray scattering techniques such as X-ray

Diffraction (XRD), X-ray Diffraction Computed Tomography (XRD-CT), Energy Dispersive X-ray Diffraction (EDXRD) and X-ray Pair Production Function (XPDF or PDF) and finally X-ray spectroscopy including hard and soft X-ray Absorption spectroscopy (hXAS and sXAS). In the last decade, the use of XRM investigation techniques for multiscale characterization of LiBs has rapidly extended becoming widespread as a demonstration of the general interest for *in situ*/ *in operando* experiments.

3.2.1 Ex situ, in situ and in operando XRM for LiBs characterization

Ex situ experiments involve the extraction of the specimen from its natural environment and its subsequent analysis. The removal of a material from an already cycled battery could damage the sample itself and/or lead to artifacts due to the high reactivity of lithium with moisture in the air, hence the use of a glovebox or a dry room is required. In addition, the analysis of the sample in environmental conditions that are far from its natural ones could give misleading information [**123,124**]. For these reasons, *in situ* and *in operando* experiments have to be privileged. However, *ex situ* results can be used in a complementary way as references for the conduction of *in situ*/*in operando* experiments and for purposes of comparison of the results.

The term *in situ* is used to indicate an experiment where the specimen is characterized in its natural physical and chemical environment but is not necessarily performing its function. This means that when LiBs are investigated after pausing the current and the voltage applied, an *in situ* experiment is taking place. *In situ* measurements show some advantages: First, reactions occurring in a specific region of interest of the sample can be instantly probed ensuring higher precision and reliability of data; second, the *in situ* approach reduces the possibility of contamination due to the high reactivity of the sample with moisture and oxygen, and diminishes the risks related to the sectioning and dismantling of the battery [**125**]. On the other hand, an *in operando* measurement occurs when the analysis takes place while the sample is performing its function. This measurement methodology continuously monitors physical, electrochemical, and micro-to-nano structural changes providing real-time operational information [**126**].

To take full advantage of an *in situ*/ *in operando* experiment, the design of the *in situ* cell becomes crucial. An optimized *in situ* cell design fits the specific technique and avoids artifacts and signals from the inactive parts of the cell. A proper cell design would avoid the undesired interference of spurious signals with the signals of actual interest [**122**]. Several examples of sophisticated *in situ* cells design can be found in literature [**127**]. Thanks to non-destructive and non-invasive *in situ*/ *in operando* monitoring techniques based on X-rays the dynamic properties and time-dependent processes can be studied thus providing a deeper insight and more accurate cause-effect relationships.

3.2.2 XRM for imaging

Among *in situ*/*in operando* X-ray imaging techniques, TXM and STXM are the most popular. Both TXM and STXM image contrast is based on the different absorption of X-rays by adjacent materials that compose

the sample, being X-ray absorption dependent on atomic number of the atoms present in the sample. The main difference between TXM and STXM lies on the way the object is illuminated. In TXM the sample is illuminated as whole with a broad X-ray beam whereas in STXM the specimen is scanned with a thin X-ray beam, instead. Since STXM requires spatial coherent light sources (which can be obtained only with synchrotron radiation sources), this type of experiment cannot be performed in an ordinary laboratory [**128**]. On the contrary, TXM experiments can be performed in both types of research infrastructures: traditional laboratory with a generator of X-ray beam and at synchrotron facilities. As specified before, synchrotron radiation offers high X-ray flux (this is particularly useful to detect low density materials such as lithium), thus achieving high temporal resolution and a better signal-to-noise ratio. STXM ensures better spatial resolution (~11 - 40 nm) when compared to TXM (~20 - 30 nm) and reduces radiation damaging to the sample. On the other hand, STXM requires considerably longer operational times due to the scanning process. The 3D rendering of the specimen can be obtained using a TXM computed tomography system and, thanks to the high energy of hard X-rays, TXM is particularly suitable for the analysis of commercial and packaged LiBs cells [**124,128**].

The aspect of safety is of fundamental importance in LiBs.[**13,14**] Therefore, every phenomenon or mechanism that jeopardizes LiBs user's health or public safety requires an in-depth examination and a fine control. Lithium dendrites growth can cause thermal runaway, capacity fade, short circuits, and may lead to catastrophic failures and even fires. Despite the seriousness of the consequences of these unwanted phenomena, their mechanisms at the microscopic level are not yet fully understood. Lithium dendrites are metallic microstructures that grow on the negative electrode during the charging process. This arises when lithium ions accumulate on the anode surface and are not absorbed by the anode itself. Even though several lithium dendrites growth models have been proposed [**124,129**], they still have many limitations, hence further experimental support is still needed. Harry *et al*. [**130**] gave a fundamental contribution with an exceptional discovery when studied lithium dendrite formation with synchrotron hard X-ray microtomography in symmetric cells with polymer electrolytes. This research demonstrated that lithium dendrites formation originates on pre-existing sub-surface structures or impurities (i.e., nucleation points) in the pre-cycled lithium foils (Figure 7)[**124**].

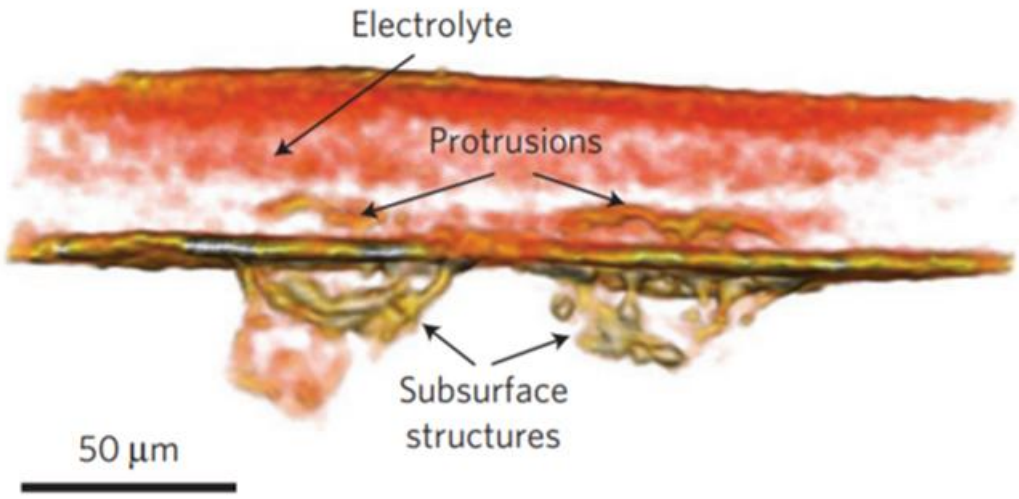

Figure 7. Reconstruction in 3D of a cell volume containing two closely spaced dendrites. The latter are indicated as protrusions overlying subsurface structures. From ref. **124**.

Cheng *et al*. [**131**] showed the ability of *in operando* TXM for studying the dynamic lithium growth mechanisms with a plastic cell design. This study revealed that the height of mossy lithium grows and shrinks more than its width, during plating/stripping processes. The effect of the current density on lithium shapes has been studied suggesting that mossy and dendritic lithium tend to grow under lower and higher current densities, respectively. Yu *et al*. [**132**] observed lithium stripping and deposition under several operating conditions such as concentration of lithium salt, current density, nature of electrolytes and additives/coatings thus deepening the knowledge of their actual relationships. This work has identified some novel Li plating morphologies such as "volcanic-Li" in $LiPF_6$-propylene carbonate electrolyte with $CsPF_6$ as additive when high current densities were traversing a lithium metal battery. This study has also shown the evolution of porosity and solidity of Li during plating. X-ray Computed Tomography has been used by Frisco *et al*. [**133**] to study the effect of temperature in lithium microstructures growth. Lower temperatures induced the formation of more voids with the consequent increase of the surface area of lithium microstructures. Gas generation within LiBs is a phenomenon that leads to the increase of internal pressure and causes mechanical stress inside the electrodes, battery swelling and gas leakage in the worst cases. This phenomenon originates from reductive and oxidative electrolyte decomposition reactions and is closely related with SEI formation [**134**]. Gas formation affects detrimentally the longevity and reliability of energy storage devices and poses serious security issues that, as a matter of fact, limit the full use of LiBs [**135**]. Sun *et al*. [**136**] visualized directly the gas and channel evolution as function of charge and discharge process in an operating LiB with a silicon anode employing synchrotron X-ray tomography (Figure 8).

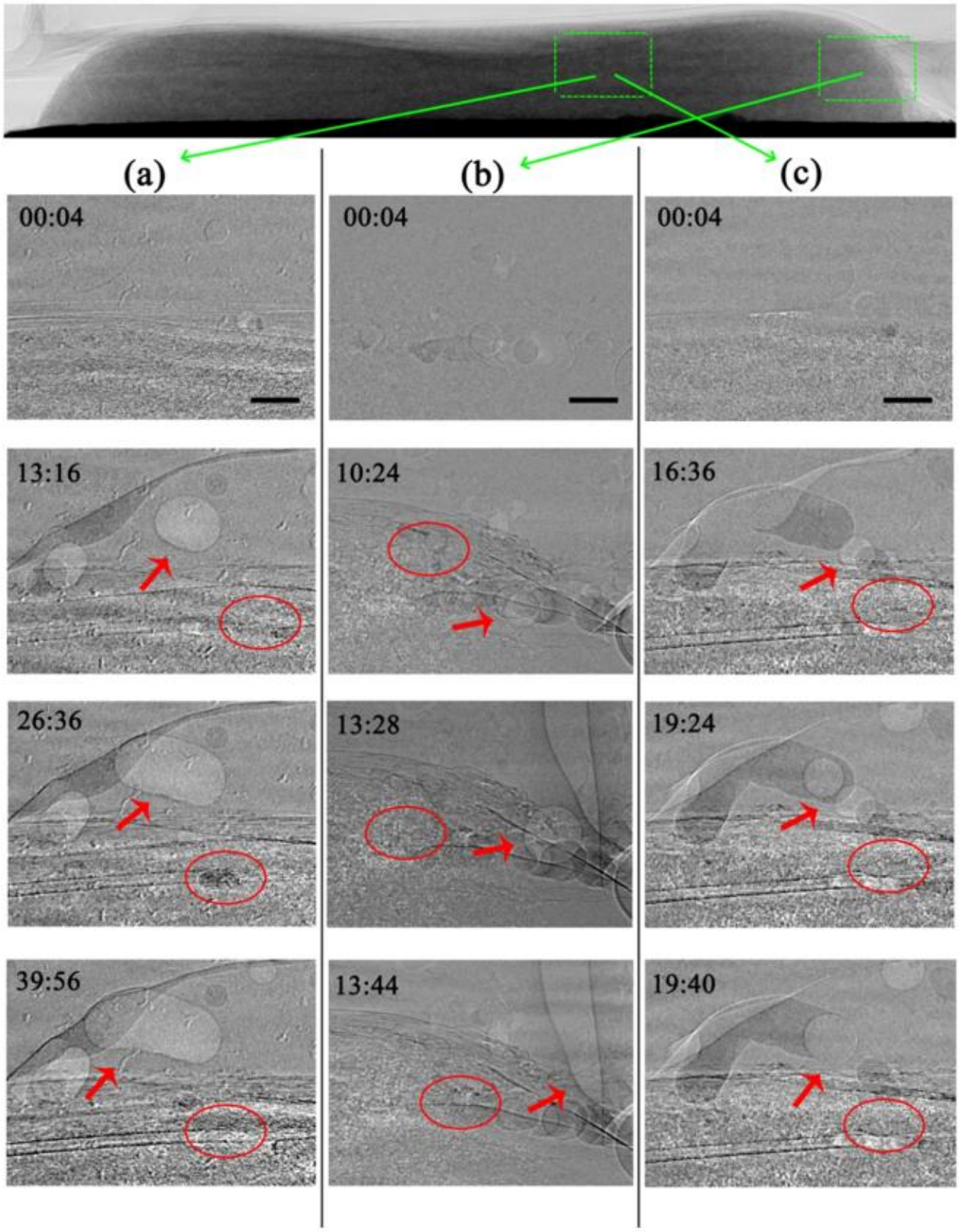

Figure 8. Series of projections showing gas movement as imaged by X-ray radiography: a–a) first discharge step, a–b) first charge step, and a–c) second discharge step. From ref. **136**.

This study has been the first in visualizing the distribution of electrochemically active electrode particles with respect to the spatial gas development. Moreover, it has been one of the first that interpret delithiation and lithiation as a process of particles activation in a step-by-step way. Gelb *et al*. [**137**] conducted a multiscale analysis of Panasonic NCR 18650-B cylindrical cells correlating 3D micro- and nano-XRM with Scanning Electron Microscopy (SEM), Focused-Ion Beam Scanning Electron Microscopy (FIB-SEM) and X-ray Dispersive X-ray Spectrometry (EDX). This study shows an interesting protocol of correlative microscopy for obtaining morphological information and quantitative evaluation of parameters at different length-scales. The work reported in ref. **137** is prone to further progresses and implementation in LiBs design. Initial low-resolution (voxel size of 22 µm) investigations were performed using laboratory X-ray microscope to characterize the general structure of the battery, its assembly, and any evident manufacturing faults. The reach of a voxel size of 1.8 µm has allowed the generation of more detailed images as shown in Figure 9.

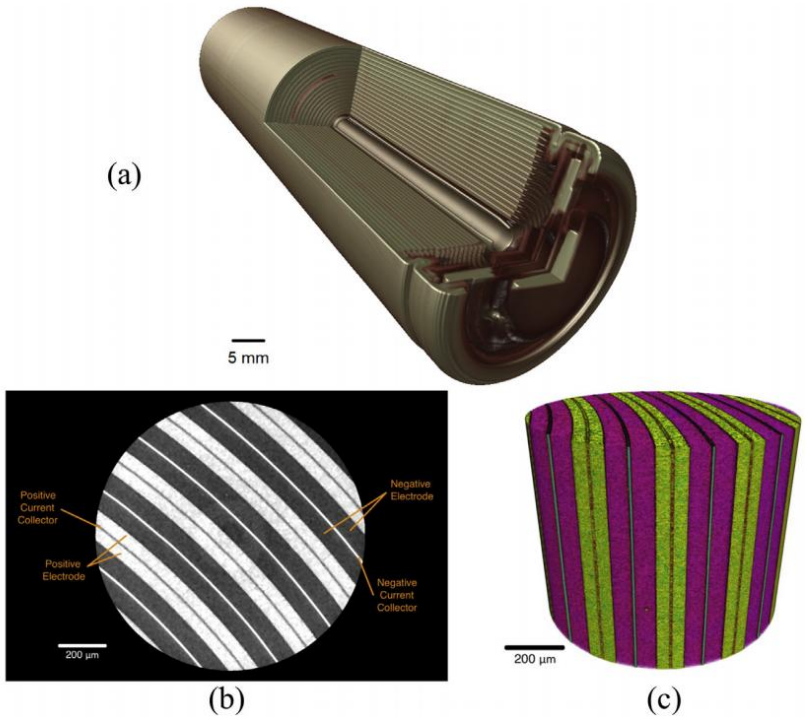

Figure 9. (a) A 3D reconstruction of the entire 18650 battery cell where the spiral architecture of the cell, inner mandrel, and cell safety devices can be observed. (b) enlarged picture of a smaller region from the center of the LiB providing insights of the layers in the spiral winding. (c) 3D volume reconstruction from the virtual slices where the lemon-yellow layers represent the positive electrode, and the magenta layers represent the negative electrode. Each layers have their respective current collectors that are sandwiched between electrode layers. It should be noted that the separator (presumably a polymer) has not been imaged, from negative electrode (presumed graphite), due to low-energy X-ray attenuation by the steel casing and metallic foils. From ref. **137**.

At the length-scale of hundreds of micron the differences between electrode layers as well as small defects may be observed. Relationships between microstructure defects and operational conditions leading to failure and capacity fade can be studied in detail with these apparatuses [**138**]. In ref. **137** sub-micron and nanoscale 3D XRM have been used to quantitatively analyze the positive electrode reaching a 130 nm voxel resolution. This technical achievement has allowed the unlocking of the information related to particle assembly, cracks, bulk defects, and porosity (Figure 10).

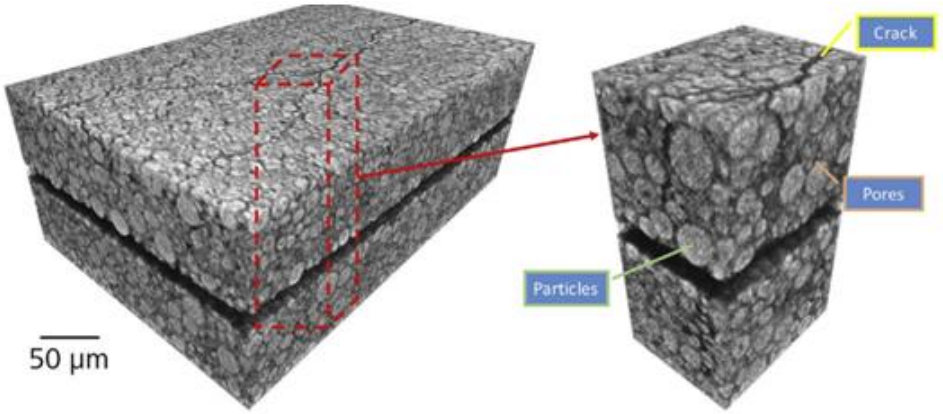

Figure 10. 3D rendering of the volume of the positive electrode layer. Particles, pores, and cracks/defects throughout the specimen thickness are evidenced in the zoomed portion on the right side. From ref. **137**.

The average porosity of each layer of active material could be calculated through slice-by-slice porosity analysis with nanoscale 3D XRM. The latter can provide information related to cracks within single particles of the positive electrode and to the percolation pathway of pores with the support of the GeoDICT software from Math2Market Gmbh (Kaiserslautern, Germany)[**139**].

3.2.3 X-ray Scattering Techniques

Crystal structures, grain size, chemical properties and phase transformations in electrodes and solid electrolyte materials can be dynamically studied using XRD. The latter is a non-destructive characterization technique based on the scattering of X-rays. When X-rays interfere with matter, diffraction patterns from crystal or partial crystalline structured materials are produced. These patterns, opportunely analyzed, provide several information regarding microstructural properties of the sample and its phases [**140**]. XRD is used for *in situ*/ *in operando* experiments to monitor average long-order structural changes of LiBs materials during charging/discharging processes and/or during temperature changes. XRD can be performed both at synchrotron facilities and in laboratory where X-ray source systems are available [**141**]. Most of XRD techniques, such as standard powder XRD, use a monochromatic X-ray beam and 2θ diffraction angles are scanned. This implies the recording of the signal coming from every part of the *in situ* cell which stands along the X-ray beam path. Such an operative characteristic conditions the use of the materials and

components in the electrochemical cell assembly. Moreover, it poses restrictions in the design of the the *in situ* cell. In contrast, EDXRD uses a polychromatic X-ray beam, and the signal is recorded at a fixed angle in order to satisfy the Bragg conditions. EDXRD allows to characterize a real battery cell with metal cases without the need of cutting or dismantling. Moreover, EDXRD offers the possibility to probe electrode materials at interfaces or near the current collector. X-rays show several advantages when compared to other probes: high penetration power combined with an excellent sensitivity of Bragg diffraction. XRD has been used by Tanim *et al*. [**142**] to study the heterogeneity of lithium plating and the associated degradation mechanisms over the cross-sectional area of a pouch cell. This approach helped to identify at the microscopic/granular level which mechanisms operate during Li plating at a local level, and provoke the loss of cell performance (global resulting effect). Yao *et al*. [**141**] presented an experimental methodology for quantifying spatial and phase heterogeneity of lithium intercalation into graphite during rapid cycling of a Gr/NCM523 cell using *in operando* EDXRD. This technique allowed to obtain a ‘‘movie’’ of lithiation and delithiation in different sections of the cell and to quantify the lithium-ion (guest species) gradients that developed in a porous graphite electrode (host species) during cycling at a 1C rate. Lithium-ion gradients in the electrodes introduce heterogeneities in the host electrode itself and render difficult the prediction of cell lifetimes. This because the presence of gradients of the guest species generate regions with different chemical composition within the intercalation electrode and different rates of cell aging in correspondence of the differently composed portions of the electrode. Steep gradients in the anode and phase specific lithium content could be revealed. LiC_6 phase showed the greatest inhomogeneity since under certain charging conditions all lithium content was localized at the surface of the electrode. This resulted in the exponential decrease of lithium content on going from electrode/electrolyte interface to the current collector with resulting scarce presence of lithium in the electrode bulk. This situation has negative effects on battery performances. These consist in the low utilization of the active material with Li plating occurring close to the electrode surface. The authors proposed the concentration profiles in the individual phases Li_xC_6 as a function of lithiation degree to be used as a benchmark for the modeling of electrochemical processes in LiBs. Raj *et al*. [**143**] used EDXRD to quantify lithium concentration and to profile the time evolution of ordered Li_xC_6 phases in solid electrodes of a LiB. Since silicon electrodes have demonstrated a high lithium capacity, the electrodes containing silicon and graphite can represent interesting alternatives to the pure graphite anodes employed in conventional LiBs. Even tough many complications are still limiting the use of silicon in LiBs, its potential led Yao and co-workers [**144**] to use *in operando* EDXRD for the investigation of lithiation/delithiation in the composite electrodes of pure silicon and graphite with 15 wt% of silicon. This study evidenced the relationship between the potential and lithiation/delithiation mechanisms. Such an information can be opportunely exploited to extend cell life.

X-ray Diffraction Computed Tomography (XRD-CT) consists in taking a series of measurements at different angles for the reconstruction of tomograms with 3D spatial crystallographic information. XRD-CT represents a promising method to provide sub-particle lithiation information and simultaneously detects the onset of Li-plating thus providing both spatial crystallographic and morphological information in a 3D fashion. Recently

Finegan *et al*. [**145**] first demonstrated that the combination of high-speed XRD and XRD-CT probes crystallographic heterogeneities within litium-ion intercalation electrodes at the spatial resolution of 1 μm with the attainment of 3D reconstructions. In Figure 11 the XRD-CT representation of the silicon−graphite electrode is reported showing a phase distribution map.[**145**]

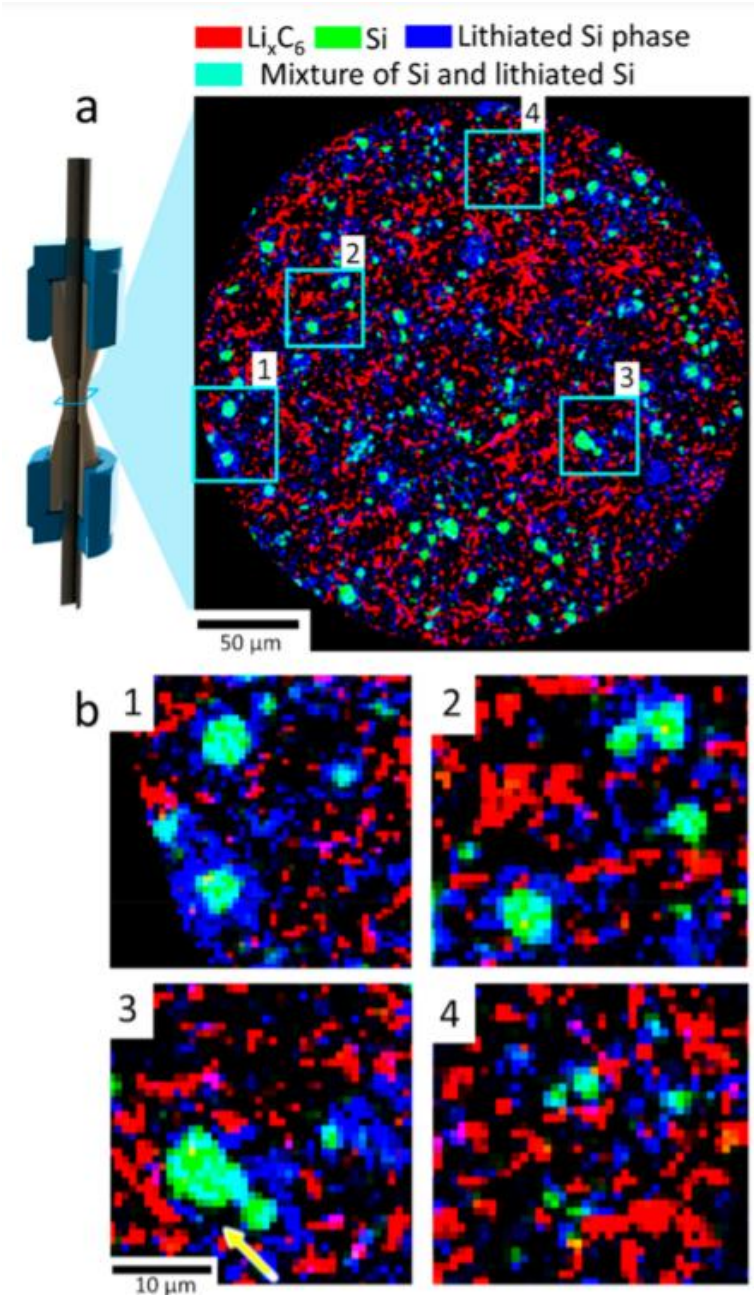

Figure 11. XRD-CT view of a silicon−graphite electrode. (a) the XRD-CT sampled slice taken at the beginning of the charge step shows a phase-distribution map of LiC_{12} (red), crystalline silicon (green), and lithium silicides Li_xSi (blue) areas. According to additive color mixing, the area with color teal represents a mixture of green (silicon) and blue (lithiated silicon). (b) Magnified regions of interest showing large particles of Li_xSi phase within crystalline silicon cores (1−3) and small Li_xSi particles (4) interspersed in the graphite matrix. From ref. **145**.

Areas of short-range order and low/no crystallinity are studied, for instance, when conversion-type electrode are involved. In these cases, XPDF or PDF become very useful to study LiBs. While XRD provides long-range average structural information, thus covering only Bragg scattering, PDF is a scattering technique that exploits the total diffracted signal (Bragg and diffuse scattering). PDF can be used to investigate materials with short range order providing local information such as the pair distribution relating to structural, morphological, and chemical transformations occurring during electrochemical reactions. A large amount of information can be obtained from XPDF data (peak position, intensity and area) such as atom-atom distance, bond length and coordination number [**146**]. *In situ* and *ex situ* PDF and Nuclear Magnetic Resonance (NMR) spectroscopy have been used in combination by Hua *et al*. [**147**] to investigate the reaction mechanism of a conversion-type carbon-coated nano-CuF_2 (CCN-CuF_2) electrode. The analysis provided local structural information during the first discharge process (Figure 12).

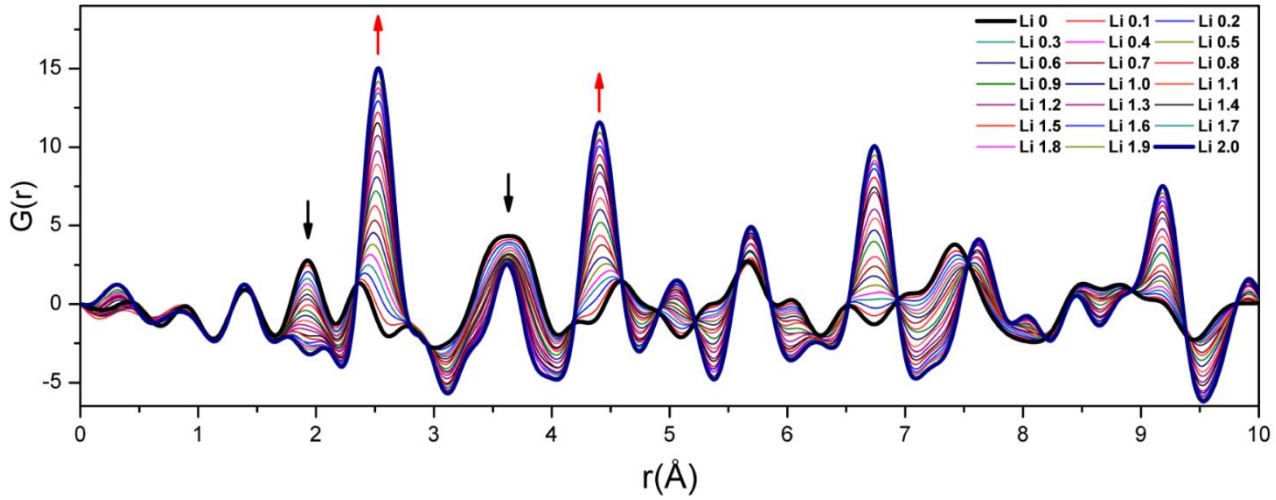

Figure 12. *In situ* PDF profiles for CCN-CuF_2 during the first discharge. The initial and end states are highlighted in bold. Black and red arrows indicate a decrease and increase in peak intensity, respectively. From ref. **147**.

The formation of metallic Cu is detected since the PDF profile for Li = 2.0 (end of the discharge) has peaks positioned at 2.6, 3.6, and 4.4 Å. Such values match the Cu−Cu distances respectively in the first, second, and third coordination shell for the face-centered cubic (FCC) Cu phase. A similar work was carried out by Wiaderek *et al*. [**148**] in which *in operando* PDF and NMR spectroscopy have been combined to gain comprehensive insights into the electrochemical reaction mechanism of high-performance iron oxyfluoride electrodes FeOF (results are shown in Figure 13).

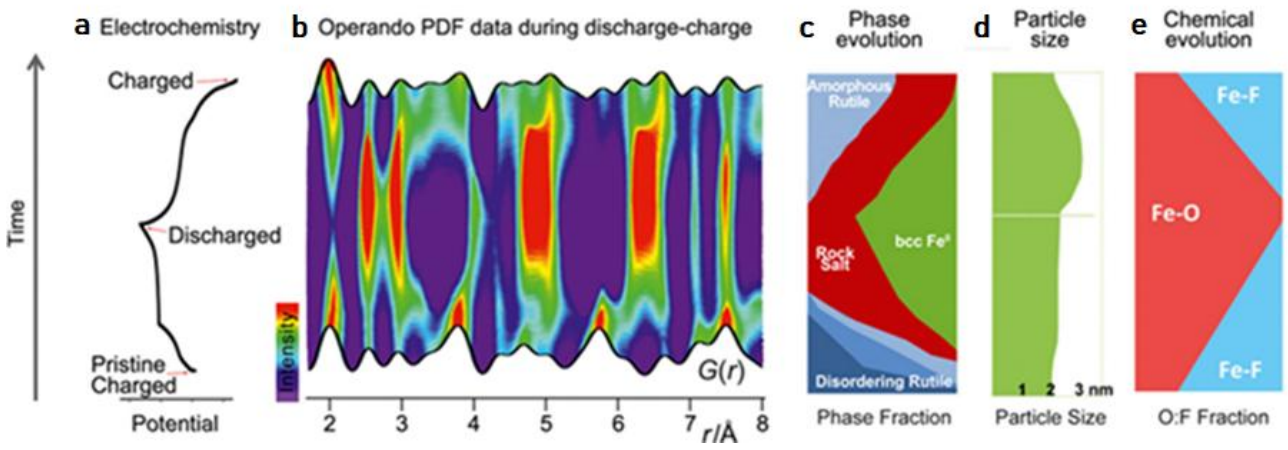

Figure 13. (a) The electrochemical lithiation (discharge) and delithiation (charge) curve of a FeOF electrode. (b) A series of *in operando* PDF data obtained at predefined reaction intervals (intercalation steps of 0.1 Li). Data fitting models show how (c) phases and (d) particle size evolve during the reactions. (e) Corresponding changes in the Fe-O and Fe-F content from the application of data fitting model. From ref. **148**.

The PDF data acquired during the initial discharge process indicate the process of conversion of FeOF to metallic Fe via the rock-salt-type intermediate phase as shown by the smooth changes in local structure and bond lengths. Even though the recharge capacity is almost the same if compared to that of initial discharge, the structure of the re-charged electrode is completely different from the initial single-phase electrode. The PDF data acquired during the recharging process suggest that the charge capacity originates from the formation of an oxide-rich rock-salt-phase and a fluoride-rich rutile phase.

3.2.4 X-ray Absorption Spectroscopy

In situ/in operando X-ray characterization for LiBs research includes XAS techniques. XAS provides information concerning elemental and chemical composition of a specimen. Since each element shows a set of characteristic absorption edges that correspond to the different binding energies of its electron, XAS is element-sensitive and suitable for probing local atomic arrangement and electronic structure of a material. XAS can be distinguished in two different energy regions relative to the absorption edges: X-ray Absorption Near Edge Structure (XANES, ~30 eV) and the Extended X-ray Absorption Fine Structure (EXAFS, above 40 eV extending to several hundred eVs) [**149**]. If XANES provides information about the oxidation states of absorbing atoms and on-site symmetry, EXAFS offers geometrical information such as bond length, coordination numbers of shells surrounding the absorbing atom and the degree of ordering [**150**]. sXAS (<3 keV) can detect K-edges of light elements such as carbon , nitrogen , sulfur and oxygen and the L-edges of transition metal elements. hXAS (> 5 keV) is used to detect K-edges of transition metal elements. Since both high intensity and coherence of the X-ray beam are required, XAS spectra must be acquired using a synchrotron radiation source. Therefore, it does not represent a routine or readily available technique [**150**]. Wang and co-workers [**151**] presented a five-dimensional imaging method combining TXM with *in situ*

XANES nanotomography to observe directly the dynamic delithiation evolution of $LiFePO_4$ particles in a working LiB. The basic principle of XANES tomography can be explained as follows. Tomography data set is acquired over a 180° rotation range, from -90° to +90°, at each photon energy step (7,102 to 7,192 eV, 2 eV per step) across the near absorption K-edge of iron in order to obtain chemical information for each voxel. Resulting spectra are then fitted as a linear combination of end-phase spectra with phase composition attributable to each voxel. This procedure provides a 3D XANES map of the sample. The results obtained by Wang and co-workers are reported in Figure 14. The evolution of the two-phase boundary separating $LiFePO_4$ and $FePO_4$ is shown in Figure 14a. The latter indicates the first stage of anisotropic migration along the y-axis in correspondence of the beginning of charging. Successively the phase boundary has an inclination toward z-axis and a curved phase boundary is observed. As long as the charging process continues, the particle becomes more delithiated and the phase boundary moves along various directions with quasi isotropic character. This mechanism is strongly related to lithium-ion diffusion paths and to the field of strain within solid [**152**]. Figure 14a shows the phase volume composition provided by 3D quantitative analysis whilst in Figure 14b the charging profile of $LiFePO_4$ is reported with the blue rectangles indicating the points at which XANES tomographic data have been collected.

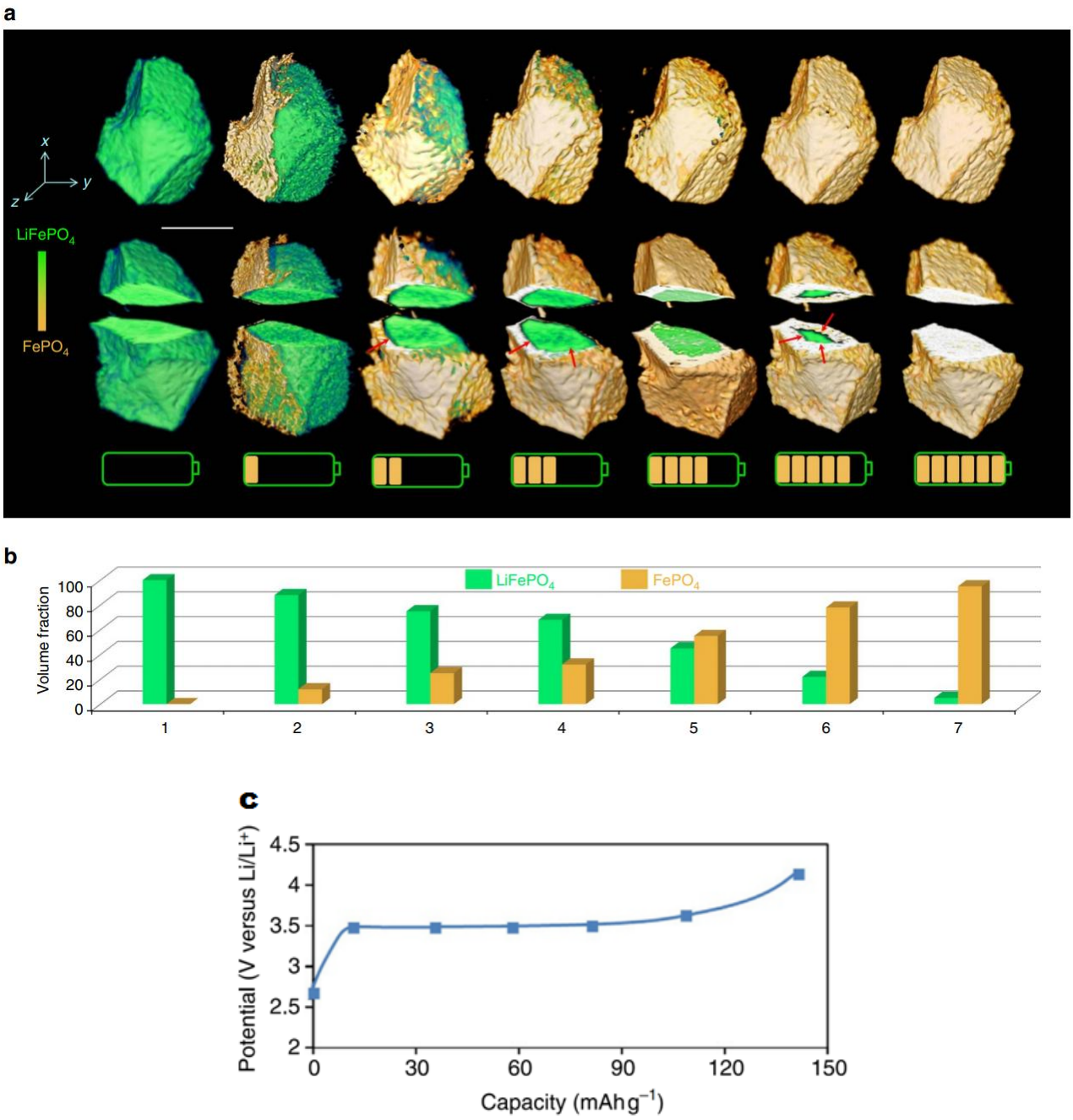

Figure 14. (a) Two-phase boundary evolution as a function of charging state. The cut-away views reveal the motion of the phase boundary within the grane with quasi isotropic features. (b) Volume fraction of $LiFePO_4$ and $FePO_4$ phases as obtained from 3D quantitative analysis. (c) Charging profile of $LiFePO_4$ battery with the blue rectangles indicating points at which XANES tomographic data sets were collected. From ref. **151**.

4. Considerations on the correlative analysis of AFM and XRM data

In general terms a correlative analysis of a given system implies that diverse characterization techniques are employed simultaneously to monitor the same portion of the system under investigation. Consequently, one of the initial problems that a correlative approach has to face is represented by the design of an experimental set-up that consents the two (or more) to-be-correlated techniques of occupying distinct (and possibly separated) spaces. For any correlatable technique the operator must consider primarily the aspects of size, weight and energy-supply requirements in the choice of corresponding stimulus-producing units and

response-collection devices. These two distinct types of units must not interphere with the analogous units of the other technique(s) in the final set-up. Therefore, the techniques operating simultaneously for a correlative analysis of a system should act independently from each other except for the synchronization of the application of the diverse stimuli. The latter achievement would allow the generation of a single time-profile for the various diverse parameters under investigation. In doing so, the resulting profiles recorded simultaneously are truly indicative of the changes in the responsive system and allow a correct correlative analysis. It is here implied that any characterization technique comprises (at least) two basic units performing the two essential functions of:

(i) production of a stimulus with controllable and known features;

(ii) collection of the response of the system (data acquisition). The response is synchronized with the stimulus thus accounting for the eventual variation (either imposed or accidental) of the stimulus

Data recording and successive elaboration are also other essential functions that should be perfomed during the operation time of a given characterization technique. This is especially important if a process of imaging formation is involved, like in case of microscopies. On the other hand, in this framework recording and elaboration do not actually represent major sources of problems since these functions are carried out by non-instrumental units, e.g. computers, the output of which depends on their memory capability, the efficacy of the running programs and the goodness of algorithms.

Other issues that are intrinsic of a correlative analysis with multiple techniques concern:

(a) the sizes of the area/volume of the system that has to be investigated simultaneously by the two (or more) techniques (extensive issue);

(b) the spatial resolution with which the area/volume of interest is scanned or monitored by the two (or more) techniques (aspects of sensitivity and detection limits of the combined techniques);

(c) the rate with which the operation of scanning/monitoring/stimulus of the portion under investigation is executed and an intelligible response is recorded (temporal resolution for the correlative analysis of the kinetics of the phenomena).

In the specific cases of the considered combination EC-AFM [a well-established one involving electrochemical and microscopical techniques with correlative purposes (*vide supra* the examples in LiBs research)] and the considerable combination AFM(EC-AFM)/XRM (a much less considered synergy that has been mainly explored in biological ambit [**153,154**]) there is ample space for continuing (or even starting from scratch) the research in the quite complicated field of LiBs. In the latter systems complicacies arise at structural and chemical levels across a very broad range of length scales (from nm to m) if unambiguous and meaningful correlations between battery structure and functionality have to be found. [**155**] In addition to that, at the practical level the operators have to consider not only the materials-related problems of the single LiB but also the questions of module assembly and pack construction with further concerns regarding connections, enclosures, control devices *etc*.. All these non-battery elements at some stages will reconduct the operators to consider the correlation of chemical, physical, morphological and structural analyses.[**1**] An example of meaningful correlative analyses of LiBs has been reported in ref. **156** in which the combination FIB/SEMt-synchrotron X-ray tomography was used for the investigation of the same specific spot of a lithium manganese oxide composite cathode. In refs. **157-162** several combinations of techniques have been considered for a correlative analytical approach and examples of such combinations are listed hereafter:

- electron backscattering diffraction/machine learning segmentation [**157**]

- confocal Raman spectroscopy/SPM [**158**]

- atom probe tomography/TEM [**159**]

- FE-SEM/TEM [**160**]

- neutron tomography/ X-ray tomography [**161**]

- digital volume correlation/synchrotron X-ray computed tomography [**162**]

For sake of simplicity, for any of the specified combinations only the corresponding reference is given in order to avoid a too dispersive description of the relative content. The reader who is interested in the investigative potentialities of a given combination for correlative purposes is redirected to the corresponding reference.

Acknowledgments

D.D., M.P. and M.R. acknowledge the University of Rome "La Sapienza" for the financial support of the ATENEO Project titled "Advanced Platform for nanoscale Electrochemical Synthesis and Characterizations based on Atomic Force Microscopy (PESCA) as tool of visualization at high spatial resolution" in the ambit of the tender GRANDI ATTREZZATURE- 2020 (prot. No. GA120173054F048C). D.D. also acknowledges the financial supports from MIUR (Project PRIN 2017 with title "Novel Multilayered and Micro-Machined Electrode Nano-Architectures for Electrocatalytic Applications" - Prot. No. 2017YH9MRK) and from the University of Rome "La Sapienza" (Project ATENEO 2019, Prot. No. RM11916B756961CA).

References

1. X. Zeng, M. Li, D.A. El-Hady, W. Alshitari, A.S. Al-Bogami, J. Lu, K. Amine "Commercialization of Lithium Battery Technologies for Electric Vehicles" *Adv. Energy Mater.* **9**(27), 1900161 (2019) [doi: 10.1002/aenm.201900161]

2. IMARC Group report "Lithium-ion Battery Market: Global Industry Trends, Share, Size, Growth, Opportunity and Forecast 2021-2026", April 2021
website: https://www.globenewswire.com/en/news-release/2021/05/06/2224199/28124/en/Global-Lithium-ion-Battery-Market-Report-2021-A-34-1-Billion-Market-in-2020-Forecast-to-2026-with-Focus-on-Consumer-Electronics-Electric-Vehicles-Energy-Storage.html

3. MRFR Report **"**Global Advanced Lithium-Ion Batteries Market Research Report: Information by Material (Anode Materials and Cathode Materials), Component (Separators, Current Collectors, Binders, Solvents and Solid-State Electrolytes), End-Use (Consumer Electronics, Automotive, Industrial and Others) and Region - Forecast till 2027", February 2021
website: https://www.marketresearchfuture.com/reports/advanced-lithium-ion-batteries-market-10123

4. G. Berckmans, M. Messagie, J. Smekens, N. Omar, L. Vanhaverbeke, J. Van Mierlo "Cost Projection of State of the Art Lithium-Ion Batteries for Electric Vehicles Up to 2030" *Energies* **10**(9), 1314 (2017) [doi: 10.3390/en10091314]

5. *Lithium-ion batteries-Advances and Applications*, G. Pistoia, Editor, Elsevier B.V., Amsterdam (2014) [doi: 10.1016/C2011-0-09658-8]

6. M. Jacoby "It's time to get serious about recycling lithium-ion batteries" *C&EN* 97(28) (2019) [website: https://cen.acs.org/materials/energy-storage/time-serious-recycling-lithium/97/i28]

7. G. Harper, R. Sommerville, E. Kendrick, L. Driscoll, P. Slater, R. Stolkin, A. Walton, P. Christensen, O. Heidrich, S. Lambert, A. Abbott, K. Ryder, L. Gaines, P. Anderson "Recycling lithium-ion batteries from electric vehicles" *Nature* **575**, 75 (2019) [doi: 10.1038/s41586-019-1682-5]

8. D. Kamath, R. Arsenault, H.C.Kim, A. Anctil "Economic and Environmental Feasibility of Second-Life Lithium-Ion Batteries as Fast-Charging Energy Storage" *Environ. Sci. Techn.* **54**(11), 6878 (2020) [doi: 10.1021/acs.est.9b05883]

9. S. Ferrari, M. Falco, A.B. Muñoz-Garcia, M. Bonomo, S. Brutti, M. Pavone, C. Gerbaldi "Solid-State Post Li Metal Ion Batteries: A Sustainable Forthcoming Reality?" *Adv. Energy Mater.* 2100785 (2021) [doi: 10.1002/aenm.202100785]

10. I. Tsiropoulos, D. Tarvydas, N. Lebedeva "Li-ion batteries for mobility and stationary storage applications" EUR 29440 EN, Publications Office of the European Union, Luxembourg, **2018**, ISBN 978-92-79-97254-6, JRC113360 [doi: 10.2760/87175]

11. J. Schnell, T. Günther, T. Knoche, C. Vieider, L. Köhler, A. Just, M. Keller, S. Passerini, G. Reinhart "All-solid-state lithium-ion and lithium metal batteries – paving the way to large-scale production**"** *J. Power Sources* **382**, 160 (2018) [doi: 10.1016/j.jpowsour.2018.02.062]

12. K.J. Huang, G. Ceder, E.A. Olivetti "Manufacturing scalability implications of materials choice in inorganic solid-state batteries" *Joule* **5**(3), 564 (2021) [doi: 10.1016/j.joule.2020.12.001]

13. K. Liu, Y. Liu, D. Lin, A. Pei, Y. Cui "Materials for lithium-ion battery safety" *Sci. Adv.* **4**(6), eaas9820 (2018) [doi: 10.1126/sciadv.aas9820]

14. Y. Chen, Y. Kang, Y. Zhao, L. Wang, J Liu, Y. Li, Z. Liang, X. He, X. Li, N. Tavajohi, B. Li "A review of lithium-ion battery safety concerns: The issues, strategies, and testing standards" *J. Energy Chem.* **59**, 83 (2021) [doi: 10.1016/j.jechem.2020.10.017]

15. B. Scrosati, J. Garche "Lithium batteries: Status, prospects and future" *J. Power Sources* **195**(9), 2419 (2010) [doi: 10.1016/j.jpowsour.2009.11.048]

16. K. Smith, A. Saxon, M. Keyser, B. Lundstrom, Ziwei Cao and A. Roc "Life prediction model for grid-connected Li-ion battery energy storage system" *2017 American Control Conference (ACC)* 4062 (2017) [doi: 10.23919/ACC.2017.7963578]

17. Y. Zhao, J. Guo "Development of flexible Li-ion batteries for flexible electronics" *InfoMat* **2**, 866 (2020) [doi: 10.1002/inf2.12117]

18. R. Xiong, Y. Zhang, J. Wang, H. He, S. Peng, M. Pecht "Lithium-Ion Battery Health Prognosis Based on a Real Battery Management System Used in Electric Vehicles" *IEEE Trans. Veh. Technol.* **68**(5), 4110 (2019) [doi: 10.1109/TVT.2018.2864688]

19. Z. Yang, J. Wu "Data Analysis and Research of Lithium-Ion Battery Based on Data Mining Technology" *J. Phys. Conf. Ser.* **1631**, 012144 (2020) [doi: 10.1088/1742-6596/1631/1/012144]

20. F.H. Gandoman, J. Jaguemont, S. Goutam, R. Gopalakrishnan, Y. Firouz, T. Kalogiannis, N. Omar, J. Van Mierlo "Concept of reliability and safety assessment of lithium-ion batteries in electric vehicles: Basics, progress, and challenges" *Appl. Energy* **251**, 113343 (2019) [doi: 10.1016/j.apenergy.2019.113343]

21. Y. Yuan, K. Amine, J. Lu, R. Shahbazian-Yassar "Understanding materials challenges for rechargeable ion batteries with *in situ* transmission electron microscopy" *Nature Commun.* **8**, 15806 (2017) [doi: 10.1038/ncomms15806]

22. G. Binnig, H. Rohrer "Scanning tunneling microscopy" *Surf. Sci.* **126**(1-3), 236 (1983) [doi: 10.1016/0039-6028(83)90716-1]

23. G. Binnig, C.F. Quate, Ch. Gerber "Atomic Force Microscope" *Phys. Rev. Lett.* **56**(9), 930 (1986) [doi: 10.1103/PhysRevLett.56.930]

24. P. Yang, Z. Bi, Y. Shang, K. Chen, Y. Liang, X. Li, G. Shang "Bimodal AFM-Based Nanocharacterization of Cycling-Induced Topographic and Mechanical Evolutions of LiMn2O4 Cathode Films" *Langmuir* **37**(21), 6406 (2021) [doi: 10.1021/acs.langmuir.1c00325]

25. J. Wu, S. Yang, W. Cai, Z. Bi, G. Shang, J. Yao "Multi-characterization of LiCoO2 cathode films using advanced AFM-based techniques with high resolution" *Sci. Rep.* **7**, 11164 (2017) [doi: 10.1038/s41598-017-11623-0]

26. S. Huang, S. Wang, G. Hu, L.Z. Cheong, C. Shen "Modulation of solid electrolyte interphase of lithium-ion batteries by LiDFOB and LiBOB electrolyte additives" *Appl. Surf. Sci.* **441**, 265 (2018) [doi: 10.1016/j.apsusc.2018.02.014]

27. S. Yang, J. Wu, B. Yan, L. Li, Y. Sun, L. Lu, K. Zeng "Nanoscale characterization of charged/discharged lithium-rich thin film cathode by scanning probe microscopy techniques" *J. Power Sources* **352**, 9 (2017) [doi: 10.1016/j.jpowsour.2017.03.082]

28. J. Domke, M. Radmacher "Measuring the elastic properties of thin polymer films with the atomic force microscope" *Langmuir* **14**(12), 3320 (1998) [doi: 10.1021/la9713006]

29. D. Passeri, A. Bettucci, A. Biagioni, M. Rossi, A. Alippi, M. Lucci, I. Davoli, S. Berezina "Quantitative measurement of indentation hardness and modulus of compliant materials by atomic force microscopy" *Rev. Sci. Instrum.* **79**, 066105 (2008) [doi: 10.1063/1.2949387]

30. Q.D. Nguyen, E.S. Oh, K.H. Chung "Nanomechanical properties of polymer binders for Li-ion batteries probed with colloidal probe atomic force microscopy" *Polym. Test.* **76**, 245 (2019) [doi: 10.1016/j.polymertesting.2019.03.025]

31. R. Garcia, R. Proksch "Nanomechanical mapping of soft matter by bimodal force microscopy" *Eur. Polym. J.* **49**(8), 1897 (2013) [doi: 10.1016/j.eurpolymj.2013.03.037]

32. K. Zeng, T. Li, T. Tian "*In situ* study of Li-ions diffusion and deformation in Li-rich cathode materials by using scanning probe microscopy techniques" *J. Phys. D: Appl. Phys.* **50**, 313001 (2017) [doi: 10.1088/1361-6463/aa7571]

33. H. Jiang, H. Peng, H. Guo, Y. Zeng, L. Li, Y. Zhang, Y. Chen, X. Chen, J. Zhang, R. Chu "Interfacial Mechanical Strength Enhancement for High-Performance ZnS Thin-Film Anodes" *ACS Appl. Mater. Interfaces* **12**, 51344 (2020) [doi: 10.1021/acsami.0c13139]

34. T.J. Young, M.A. Monclus, T.L. Burnett, W.R. Broughton, S.L. Ogin, "The use of the PeakForce^{TM} quantitative nanomechanical mapping AFM-based method for high-resolution Young's modulus measurement of polymers" *Meas. Sci. Technol.* **22**, 125703 (2011) [doi: 10.1088/0957-0233/22/12/125703]

35. Z. Zhang, K. Smith, R. Jervis, P.R. Shearing, T.S. Miller, D.J.L. Brett "*Operando* Electrochemical Atomic Force Microscopy of Solid−Electrolyte Interphase Formation on Graphite Anodes: The Evolution of SEI Morphology and Mechanical Properties" *ACS Appl. Mater. Interfaces* **12**, 35132 (2020) [doi: 10.1021/acsami.0c11190]

36. R. Hiesgen, S. Sörgel, R. Costa, L. Carlé, I. Galm, N. Cañas, B. Pascucci, K.A. Friedrich "AFM as an analysis tool for high-capacity sulfur cathodes for Li–S batteries" *Beilstein J. Nanotechnol.* **4**, 611 (2013) [doi: 10.3762/bjnano.4.68]

37. A. Sikora, L. Bednarz "Mapping of mechanical properties of the surface by utilization of torsional oscillation of the cantilever in atomic force microscopy" *Cent. Eur. J. Phys.* **9**(2), 372 (2011) [doi: 10.2478/s11534-010-0127-4]

38. A. Sikora, M. Woszczyna, M. Friedemann, F.J. Ahlers, M. Kalbac "AFM diagnostics of graphene-based quantum Hall devices" *Micron* **43**(2-3), 479(2012) [doi: 10.1016/j.micron.2011.11.010]

39. M. Michalska, L. Lipińska, A. Sikora, D. Ziółkowska, K.P. Korona, M. Andrzejczuk "Structural and morphological studies of manganese-based cathode materials for lithium ion batteries" *J. Alloys Compd.* **632**, 256 (2015) [doi: 10.1016/j.jallcom.2014.12.266]

40. M. Reggente, M. Natali, D. Passeri, M. Lucci, I. Davoli, G. Pourroy, P. Masson, H. Palkowski, U. Hangen, A. Carradò, M. Rossi "Multiscale mechanical characterization of hybrid Ti/PMMA layered materials" *Colloids Surf. A* **532**, 244 (2017) [doi: 10.1016/j.colsurfa.2017.05.011]

41. S.C. Nagpure, B. Bhusan, S. Babu, G. Rizzoni "Scanning spreading resistance characterization of aged Li-ion batteries using atomic force microscopy" *Scr. Mater.* **60**(11), 933 (2009) [doi: 10.1016/j.scriptamat.2009.01.033]

42. J. Op de Beeck, N. Labyedh, A. Sepúlveda, V. Spampinato, A. Franquet, T. Conard, P.M. Vereecken, W. Vandervorst, U. Celano "Nanoscale electrochemical response of lithium-ion cathodes: a combined study using C-AFM and SIMS" *Beilstein J. Nanotechnol.* **9**, 1623 (2018) [doi: 10.3762/bjnano.9.154]

43. Y. Chen, Y. Niu, C. Lin, J. Li, Y. Lin, G.G. Xu, R.E. Palmer, Z. Huang "Insight into the intrinsic mechanism of improving electrochemical performance via constructing the preferred crystal orientation in lithium cobalt dioxide" *Chem. Eng. J.* **399**, 125708 (2020) [doi: 10.1016/j.cej.2020.125708]

44. M. Nonnenmacher, M.P. O'Boyle, H.K. Wickramasinghe "Kelvin probe force microscopy" *Appl. Phys. Lett.* **58**, 2921-2923 (1991) [doi: 10.1063/1.105227]

45. S.C. Nagpure, B. Bhushan, S.S. Babu "Surface potential measurement of aged Li-ion batteries using Kelvin probe microscopy" *J. Power Sources* **196**(3), 1508 (2011) [doi: 10.1016/j.jpowsour.2010.08.031]

46. A. Buchheit, M. Hoffmeyer, B. Teßmer, K. Neuhaus "Characterization of the Particle-Polymer Interface in Dual-Phase Electrolytes by Kelvin Probe Force Microscopy" *J. Electrochem. Soc.* **168**, 010531 (2021) [doi: 10.1149/ 1945-7111/abda59]

47. H. Masuda, N. Ishida, Y. Ogata, D. Ito, D. Fujita "Internal potential mapping of charged solid-state-lithium ion batteries using *in situ* Kelvin probe force microscopy" *Nanoscale* **9**, 893 (2017) [doi: 10.1039/c6nr07971g]

48. Y. Yamaguchi, M. Shiota, Y. Nakayama, N. Hirai, S. Hara, "Combined *in situ* EC-AFM and CV measurement study on lead electrode for lead-acid batteries" *J. Power Sources* **93**(1-2), 104 (2001) [doi: 10.1016/S0378-7753(00)00554-1]

49. K.A. Hirasawa, T. Sato, H. Asahina, S. Yamaguchi, S. Mori "*In situ* electrochemical atomic force microscope study on graphite electrodes" *J. Electrochem. Soc.* **144**, L81 (1997) [doi: 10.1149/1.1837560]

50. R. Vidu, F.T. Quinlan, P. Stroeve "Use of *In Situ* Electrochemical Atomic Force Microscopy (EC-AFM) to Monitor Cathode Surface Reaction in Organic Electrolyte" *Ind. Eng. Chem. Res.* **41**(25), 6546 (2002) [doi: 10.1021/ie020519z]

51. J.V. Macpherson, P.R. Unwin "Combined Scanning Electrochemical-Atomic Force Microscopy" *Anal. Chem.* **72**(2), 276 (2000) [doi: 10.1021/ac990921w]

52. A. Kueng, C. Kranz, B. Mizaikoff, A. Lugstein, E. Bertagnolli "Combined scanning electrochemical atomic force microscopy for tapping mode imaging" *Appl. Phys. Lett.* **82**(10), 1592 (2003) [doi: 10.1063/1.1559652]

53. T. Kouzeki, S. Tatezono, H. Yanagi "Electrochromism of Orientation-Controlled Naphthalocyanine Thin Films" *J. Phys. Chem.* **100**(51), 20097 (1996) [doi: 10.1021/jp962307j]

54. M. Reggente, D. Passeri, M. Rossi, E. Tamburri, M.L. Terranova "Electrochemical atomic force microscopy: *In situ* monitoring of electrochemical processes" *AIP Conf. Proc.* **1873**, 020009 (2017) [doi: 10.1063/1.4997138]

55. L.A. Bottomley "Scanning Probe Microscopy" *Anal. Chem.* **70**(12), 425R (1998) [doi: 10.1021/a1980011o]

56. A.A. Gewirth, B.K. Niece "Electrochemical Applications of *In Situ* Scanning Probe Microscopy" *Chem. Rev.* **97**(4), 1129 (1997) [doi: 10.1021/cr960067y]

57. H. Li, S. Guo, H. Zhou "In-situ/*operando* characterization techniques in lithium-ion batteries and beyond" *J. Energy Chem.* **59**, 191 (2021) [doi: 10.1016/j.jechem.2020.11.020]

58. S. Wang, Q. Liu, C. Zhao, F. Lv, X. Qin, H. Du, F. Kang, B. Li "Advances in Understanding Materials for Rechargeable Lithium Batteries by Atomic Force Microscopy" *Energy Environ. Mater.* **1**(1), 28 (2018) [doi: 10.1002/eem2.12002]

59. M. Kitta, H. Sano "Determination of solid electrolyte interphase formation mechanism on negative electrode surface in Li-O-2 battery electrolyte by *operando* electrochemical atomic force microscopy observation" *Appl. Surf. Sci.* **528**, 146997 (2020) [doi: 10.1016/j.apsusc.2020.146997]

60. R. Zhao, S. Wang, D. Liu, Y. Liu, X. Lv, X. Zeng, B. Li "Effect of Fluoroethylene Carbonate on Solid Electrolyte Interphase Formation of the SiO/C Anode Observed by *In Situ* Atomic Force Microscopy" *ACS Appl. Energy Mater.* **4**(1), 492 (2021) [doi: 10.1021/acsaem.0c02399]

61. M. Kitta "*In-Operando* Detection of the Physical Property Changes of an Interfacial Electrolyte during the Li-Metal Electrode Reaction by Atomic Force Microscopy" *Langmuir* **36**(33), 9701 (2020) [doi: 10.1021/acs.langmuir.0c00986]

62. P. Yang, Z. Bi, Y. Shang, K. Chen, Y. Liang, X. Li, G. Shang "Bimodal AFM-Based Nanocharacterization of Cycling-Induced Topographic and Mechanical Evolutions of LiMn2O4 Cathode Films" *Langmuir* **37**(21), 6406 (2021) [doi: 10.1021/acs.langmuir.1c00325]

63. N. Boaretto, I. Garbayo, S. Valiyaveettil-SobhanRaj, A. Quintela, C. Li, M. Casas-Cabanas, F.Aguesse "Lithium solid-state batteries: State-of-the-art and challenges for materials, interfaces and processing" *J. Power Sources* **502**, 229919 (2021) [doi: 10.1016/j.jpowsour.2021.229919]

64. Y.X. Song, Y. Shi, J. Wan, B. Liu, L.J. Wan, R. Wen "Dynamic Visualization of Cathode/Electrolyte Evolution in Quasi-Solid-State Lithium Batteries" *Adv. Energy Mater.* **10**(25), 2000465 (2020) [doi: 10.1002/aenm.202000465]

65. P. Ghigna, E. Quartarone "*Operando* X-ray absorption spectroscopy on battery materials: a review of recent developments" *J. Phys. Energy* **3**, 032006 (2021) [doi: 10.1088/2515-7655/abf2db]

66. D.S. Eastwood, P.M. Bayley, H.J. Chang, O.O. Taiwo, J. Vila-Comamala, D.J.L. Brett, C. Rau, P.J. Withers, P.R. Shearing, C.P. Grey, P.D. Lee "Three-dimensional characterization of electrodeposited lithium microstructures using synchrotron X-ray phase contrast imaging" *Chem. Commun.* **51**, 266 (2015) [doi: 10.1039/C4CC03187C]

67. H. Fujimoto, H. Kiuchi, S. Takagi, K. Shimoda, K. Okazaki, Z. Ogumi, T. Abe "Assessing Reaction Mechanisms of Graphite Negative Electrodes Based on *Operando* Synchrotron Radiation Diffraction Data" *J. Electrochem. Soc.* **168**, 040509 (2021) [doi: 10.1149/1945-7111/abf181]

68. K.Suzuki , Y. Otsuka, N. Tsuji, K. Hoshi, Y. Sakurai, H. Sakurai "Identifying the Degradation Mechanism in Commercial Lithium Rechargeable Batteries via High-Energy X-ray Compton Scattering Imaging" *Appl. Sci.* **10**(17), 5855 (2020) [doi:10.3390/app10175855]

69. D. Petz, M.J. Mühlbauer, V. Baran, A. Schökel, V. Kochetov, M. Hofmann,V. Dyadkin, P. Staron, G. Vaughan, U. Lienert, P. Müller-Buschbaum, A. Senyshyn "Lithium distribution and transfer in high-power 18650-type Li-ion cells at multiple length scales" *Energy Storage Mater.* **41**, 546 (2021) [doi: 10.1016/j.ensm.2021.06.028]

70. T. Li, X. Zhou, Y. Cui, M.L. Meyerson, J.A. Weeks, C. Buddie Mullins, V. De Andrade, F. De Carlo, Y. Liu, L. Zhu **"***In Situ* Characterization of Dynamic Morphological and Phase Changes of Selenium-doped Germanium Using a Single Particle Cell and Synchrotron Transmission X-ray Microscopy" *ChemSusChem* **14**, 1370 (2021) [doi: 10.1002/cssc.202002776**]**

71. H. Fathiannasab, A.G. Kashkooli, T. Li, L. Zhu, Z. Chen "Three-Dimensional Modeling of All-Solid-State Lithium-Ion Batteries Using Synchrotron Transmission X-ray Microscopy Tomography" *J. Electrochem. Soc.* **167**(10), 100558 (2020) [doi: 10.1149/1945-7111/ab9380]

72. M.B. Dixit, A. Verma, W. Zaman, X. Zhong, P. Kenesei, J.S.Park, J. Almer, P.P. Mukherjee, K.B. Hatzell **"**Synchrotron Imaging of Pore Formation in Li Metal Solid-State Batteries Aided by Machine Learning**"** *ACS Appl. Energy Mater.* **3**(10), 9534 (2020) [doi: 10.1021/acsaem.0c02053]

73. H. Charalambous, D.P.Abraham,A.R. Dunlop, S.E.Trask, A.N. Jansen, T.R.Tanim, P.R.Chinnam, A.M. Colclasure, W. Xu, A.A.Yakovenko, O. J. Borkiewicz, L.C. Gallington, U. Ruett, K.M.Wiaderek, Y. Ren "Revealing causes of macroscale heterogeneity in lithium ion pouch cells via synchrotron X-ray diffraction" *J. Power Sources* **507**, 230253 (2021) [doi: 10.1016/j.jpowsour.2021.230253]

74. T.Y. Chen, S.Y. Wang, C.H. Kuo, S.C. Huang, M.H. Lin, C.H. Li, H.Y. Yi, T. Chen, C.C. Wang, Y.F. Liao, C.C. Lin, Y.M. Chang, J.W. Yeh,S.J. Lin, T.Y. Chen, H.Y. Chen "*In operando* synchrotron X-ray studies of a novel spinel $(Ni_{0.2}Co_{0.2}Mn_{0.2}Fe_{0.2}Ti_{0.2})_3O_4$ high-entropy oxide for energy storage applications" *J. Mater. Chem. A* **8**, 21756 (2020) [doi: 10.1039/D0TA06455F]

75. C. Shen, G. Hu, L.Z. Cheong, S. Huang, J.G. Zhang, D. Wang "Direct Observation of the Growth of Lithium Dendrites on Graphite Anodes by *Operando* EC-AFM" *Small Methods* **2**(2), 1700298 (2018) [doi: 10.1002/smtd.201700298]

76. H. Zhang, D. Wang, C. Shen "*In situ* EC-AFM and ex-situ XPS characterization to investigate the mechanism of SEI formation in highly concentrated aqueous electrolyte for Li-ion batteries" *Appl. Surf. Sci.* **507**, 145059 (2020) [doi: 10.1016/j.apsusc.2019.145059]

77. W. J. Legerstee, M. Boekel, S. Boonstra, E.M. Kelder "Scanning Probe Microscopy Facility for *Operando* Study of Redox Processes on Lithium ion Battery Electrodes" *Front. Chem.* **9**, 505876 (2021) [doi: 10.3389/fchem.2021.505876]

78. D. Chen, S. Huang, L. Zhong, S. Wang, M. Xiao, D. Han, Y. Meng "*In Situ* Preparation of Thin and Rigid COF Film on Li Anode as Artificial Solid Electrolyte Interphase Layer Resisting Li Dendrite Puncture" *Adv. Funct. Mater.* **30**(7), 1907717 (2020) [doi: 10.1002/adfm.201907717]

79. S. Huang, L.Z. Cheong, S. Wang, D. Wang, C. Shen "*In situ* study of surface structure evolution of silicon anodes by electrochemical atomic force microscopy" *Appl. Surf. Sci.* **452**, 67 (2018) [doi: 10.1016/j.apsusc.2018.05.020]

80. K.Guo, R. Kumar, X. Xiao, B.W. Sheldon, H. Gao "Failure progression in the solid electrolyte interphase (SEI) on silicon electrodes" *Nano Energy* **68**, 104257 (2020) [doi: 10.1016/j.nanoen.2019.104257]

81. D. Uxa, B. Jerliu, E. Hüger, L. Dörrer, M. Horisberger, J. Stahn , H. Schmidt "On the Lithiation Mechanism of Amorphous Silicon Electrodes in Li-Ion Batteries" *J. Phys. Chem. C* **123**(36), 22027 [doi: 10.1021/acs.jpcc.9b06011]

82. S. Benning, C. Chen**,** R.A. Eichel, P.H.L. Notten, F. Hausen "Direct Observation of SEI Formation and Lithiation in Thin-Film Silicon Electrodes via *in Situ* Electrochemical Atomic Force Microscopy" ACS Appl. Energy Mater. **2**(9), 6761 (2019) [doi: 10.1021/acsaem.9b01222]

83. Y. Shi, J. Wan, J.Y. Li, X.C. Hu, S.Y. Lang, Z.Z. Shen, G. Li, H.J. Yan, K.C. Jiang, Y.G. Guo, R.Wen, L.J. Wan "Elucidating the interfacial evolution and anisotropic dynamics on silicon anodes in lithium-ion batteries" Nano Energy **61**, 304 (2019) [doi: 10.1016/j.nanoen.2019.04.074]

84. R.C. Longo, L.E. Camacho-Forero, P.B. Balbuena "Li2S growth on graphene: Impact on the electrochemical performance of Li-S batteries" *J. Chem. Phys.* **152**(1), 014701 [doi: 10.1063/1.5135304]

85. C. Shen, S. Wang, Y. Jin, W.Q. Han "*In Situ* AFM Imaging of Solid Electrolyte Interfaces on HOPG with Ethylene Carbonate and Fluoroethylene Carbonate-Based Electrolytes" *ACS Appl. Mater. Interfaces* **7**(45), 25441 (2015) [doi: 10.1021/acsami.5b08238]

86. R. Wen, M. Hong, H.R. Byon "*In Situ* AFM Imaging of Li-O-2 Electrochemical Reaction on Highly Oriented Pyrolytic Graphite with Ether-Based Electrolyte" *J. Am. Chem. Soc.* **135**(29), 10870 (2013) [doi: 10.1021/ja405188g]

87. S.K. Jeong, M. Inaba, T. Abe, Z. Ogumi, "Surface Film Formation on Graphite Negative Electrode in Lithium-Ion Batteries - AFM Study in an Ethylene Carbonate-Based Solution" *J. Electrochem. Soc.* **148**(9), A989 (2001) [doi:10.1149/1.1387981]

88. S. Leroy, F. Blanchard, R. Dedryvère, H. Martinez, B. Carré, D. Lemordant, D. Gonbeau "Surface film formation on a graphite electrode in Li-ion batteries: AFM and XPS study" *Surf. Interface Anal.* **37**(10), 773 (2005) [doi:10.1002/sia.2072]

89. D. Aurbach, M. Koltypin, H. Teller "*In Situ* AFM Imaging of Surface Phenomena on Composite Graphite Electrodes during Lithium Insertion" *Langmuir* **18**(23), 9000 (2002) [doi: 10.1021/la020306e]

90. S.K. Jeong, M. Inaba, Y. Iriyama, T. Abe, Z. Ogumi "AFM study of surface film formation on a composite graphite electrode in lithium-ion batteries" *J. Power Sources* **119–121**, 555 (2003) [doi:10.1016/S0378-7753(03)00288-X]

91. S.K. Jeong, M. Inaba, Y. Iriyama, T. Abe, Z. Ogumi "Surface film formation on a graphite negative electrode in lithium-ion batteries: AFM study on the effects of co-solvents in ethylene carbonate-based solutions" *Electrochim. Acta* **47**(12), 1975 (2002) [doi:10.1016/S0013-4686(02)00099-3]

92. Y. Domi, M. Ochida, S. Tsubouchi, H. Nakagawa, T. Yamanaka, T. Doi, T. Abe, Z. Ogumi "*In Situ* AFM Study of Surface Film Formation on the Edge Plane of HOPG for Lithium-Ion Batteries" *J. Phys Chem. C* **115**(51), 25484 (2011)[doi:10.1021/jp2064672]

93. X. Deng, X.R. Liu, H.J. Yan, D. Wang, L.J. Wan "Morphology and modulus evolution of graphite anode in lithium ion battery: An *in situ* AFM investigation" *Sci. China Chem.* **57**(1), 178 (2014) [doi: 10.1007/s11426-013-4988-4]

94. S.Yu. Luchkin, S.A. Lipovskikh, N.S. Katorova, A.A. Savina, A.M. Abakumov, K.J. Stevenson "Solid-electrolyte interphase nucleation and growth on carbonaceous negative electrodes for Li-ion batteries visualized with *in situ* atomic force microscopy" *Sci. Rep.* **10**, 8550 (2020) [doi: 10.1038/s41598-020-65552-6]

95. G. Zampardi, S. Klink, V. Kuznetsov, T. Erichsen, A. Maljusch, F. La Mantia, W. Schuhmann, E. Ventosa "Combined AFM/SECM Investigation of the Solid Electrolyte Interphase in Li-Ion Batteries" *ChemElectroChem* **2**, 1607 (2015) [doi: 10.1002/celc.201500085]

96. J. Hui, Z.T. Gossage, D. Sarbapalli, K. Hernández-Burgos, J. Rodríguez-López "Advanced Electrochemical Analysis for Energy Storage Interfaces" *Anal. Chem.* **91**(1), 60 (2019) [doi: 10.1021/acs.analchem.8b05115]

97. G. Bussetti, R. Yivlialin, D. Alliata, A. Li Bassi, C. Castiglioni, M. Tommasini, C.S. Casari, M. Passoni, P. Biagioni, F. Ciccacci, L. Duò "Disclosing the Early Stages of Electrochemical Anion Intercalation in Graphite by a Combined Atomic Force Microscopy/Scanning Tunneling Microscopy Approach" *J. Phys. Chem. C* **120**(11), 6088 (2016) [doi: 10.1021/acs.jpcc.6b00407]

98. G. Bussetti, M. Campione, A. Bossi, R. Yivlialin, L. Duò "Anion intercalated graphite: a combined electrochemical and tribological investigation by *in situ* AFM" *J. Microscopy* **280**(3), 222 (2020) [doi:10.1111/jmi.12927]

99. M. Koltypin, Y.S. Cohen, B. Markovsky, Y. Cohen, D. Aurbach "The study of lithium insertion–deinsertion processes into composite graphite electrodes by *in situ* atomic force microscopy (AFM)" *Electrochem. Commun.* **4**(1), 17 (2002) [doi:10.1016/S1388-2481(01)00264-8]

100. F.P. Campana, R. Kötz, J. Vetter, P. Novák, H. Siegenthaler "*In situ* atomic force microscopy study of dimensional changes during Li+ ion intercalation/de-intercalation in highly oriented pyrolytic graphite" *Electrochem. Commun.* **7**(1), 107 (2005) [doi: 10.1016/j.elecom.2004.11.015]

101. Z. Liu, Z. Bi, Y. Shang, Yn Liang, P. Yang, X. Li, C. Zhang, G. Shang "Visualization of Electrochemical Cycling-Induced Dimension Change in LiMn2O4 Nanoparticles by High-Speed Atomic Force Microscopy" *Langmuir* **36**(17), 4689 (2020) [doi: 10.1021/acs.langmuir.0c00490]

102. J. Wu, W. Cai, G. Shang "*In situ* Electrochemical-AFM Study of LiFePO4 Thin Film in Aqueous Electrolyte" *Nanoscale Res. Lett.* **11**, 223 (2016) [doi: 10.1186/s11671-016-1446-1]

103. M. Simolka, H. Kaess, K.A. Friedrich "Comparison of fresh and aged lithium iron phosphate cathodes using a tailored electrochemical strain microscopy technique" *Beilstein J. Nanotechn.* **11**, 583 (2020) [doi: 10.3762/bjnano.11.46]

104. K. Mahankali, N.K. Thangavel, L.M.R. Arava "*In Situ* Electrochemical Mapping of Lithium–Sulfur Battery Interfaces Using AFM–SECM" *Nano Lett.* **19**(8), 5229 (2019) [doi: 10.1021/acs.nanolett.9b01636]

105. Y.X. Song, J. Wan, H.J. Guo, Y. Shi, X.C. Hu, B. Liu, H.J. Yan, R. Wen, L.J. Wan "Insights into evolution processes and degradation mechanisms of anion-tunable interfacial stability in all-solid-state lithium-sulfur batteries" *Energy Storage Mater.* **41**, 642 (2021) [doi: 10.1016/j.ensm.2021.06.031]

106. J. Hu, L. Li, E. Hu, S. Chae, H. Jia, T. Liu, B. Wu, Y. Bi, K. Amine, C. Wang, J. Zhang, J. Tao, J. Xiao "Mesoscale-architecture-based crack evolution dictating cycling stability of advanced lithium ion batteries" *Nano Energy* **79**, 105420 (2021) [doi: 10.1016/j.nanoen.2020.105420]

107. A. Clémençon, A.T. Appapillai, S. Kumar, Y. Shao-Horn "Atomic force microscopy studies of surface and dimensional changes in LixCoO2 crystals during lithium de-intercalation" *Electrochim. Acta* **52**(13), 4572 (2007) [doi: 10.1016/j.electacta.2006.12.076]

108. Y.S. Cohen, D. Aurbach "Surface films phenomena on vanadium-pentoxide cathodes for Li and Li-ion batteries: *in situ* AFM imaging" *Electrochem. Commun.* **6**(6), 536 (2004) [doi: 10.1016/j.elecom.2004.03.014]

109. J. Światowska-Mrowiecka, V. Maurice, L. Klein, P. Marcus "Nanostructural modifications of V2O5 thin films during Li intercalation studied *in situ* by AFM" *Electrochem. Commun.* **9**(9), 2448 (2007)[doi:10.1016/j.elecom.2007.07.008]

110. R. Vidu, P. Stroeve "Improvement of the Thermal Stability of Li-Ion Batteries by Polymer Coating of LiMn2O4" *Ind. Eng. Chem. Res.* **43**(13), 3314 (2004) [doi: 10.1021/ie034085z]

111. Z. Liu, Z. Bi, Y. Shang, Y. Liang, P. Yang, X. Li, C. Zhang, G. Shang "Development of electrochemical high-speed atomic force microscopy for visualizing dynamic processes of battery electrode materials, *Rev. Sci. Instrum.* **91**, 103701 (2020) [doi:10.1063/5.0024425]

112. P.P. Paul, E.J. McShane, A.M. Colclasure, N. Balsara, D.E. Brown, C. Cao, B.R. Chen, P.R. Chinnam, Y. Cui, E.J. Dufek, D.P. Finegan, S. Gillard, W. Huang, Z.M. Konz, R. Kostecki, F. Liu, S. Lubner, R. Prasher, M.B. Preefer, J. Qian, M.TR. Fonseca Rodrigues, M. Schnabel, S.B. Son, V. Srinivasan, H.G. Steinrück, T.R. Tanim, M.F. Toney, W. Tong, F. Usseglio-Viretta, J.Wan, M. Yusuf, B.D. McCloskey, J.N. Weker "A Review of Existing and Emerging Methods for Lithium Detection and Characterization in Li-Ion and Li-Metal Batteries" *Adv. Energy Mater.* **11**, 2100372 (2021) [doi: 10.1002/aenm.202100372]

113. M.S. Whittigham "Ultimate Limits to Intercalation Reactions for Lithium Batteries" *Chem. Rev.* **114**(23), 11414 (2014) [doi: 10.1021/cr5003003]

114. P.G. Bruce, B. Scrosati, J.M. Tarascon **"**Nanomaterials for Rechargeable Lithium Batteries" *Angew. Chem. Int. Ed.* **47**, 2930 (2008) [doi: 10.1002/anie.200702505]

115. Asylum Glovebox Solutions for Research AFMs, https://afm.oxinst.com/assets/uploads/products/asylum/documents/Turnkey-Glovebox-Solutions-for-Asylum-Research-AFMs-Data-Sheet.pdf

116. D. Sayre, H.N. Chapman "X-ray microscopy" *Acta Cryst.* **A51**, 237 (1995) [doi: 10.1107/S0108767394011803]

117. S. Carmignato, W. Dewulf, R. Leach, *Industrial X-Ray Computed Tomography*, Springer International Publishing AG, p.369, Cham (2018) [doi: 10.1007/978-3-319-59573-3]

118. K. Orhan, *Micro-computed Tomography (micro-CT) in Medicine and Engineering*, Springer International Publishing AG, p.437, Cham (2020) [doi: 10.1007/978-3-030-16641-0]

119. S.R. Stock, *MicroComputed Tomography-Methodology and Applications*, CRC Press, p. 389, Boca Raton (2020)

120. G. Wang, Y. Zhang, X. Ye, X. Mou, *Machine Learning for Tomographic Imaging (IPEM-IOP Series in Physics and Engineering in Medicine and Biology)*, IOP Publishing, p. 410, Bristol (2020) [doi: 10.1088/978-0-7503-2216-4]

121. H. Dejea, P. Garcia-Canadilla, A.C. Cook, E. Guasch, M. Zamora, F. Crispi, M. Stampanoni, B. Bijnens, A. Bonnin, "Comprehensive Analysis of Animal Models of Cardiovascular Disease using Multiscale X-Ray Phase Contrast Tomography" *Sci. Rep.* **9**, 6996 (2019) [doi: 10.1038/s41598-019-43407-z]

122. S.M. Bak, Z. Shadike, R. Lin, X. Yu, X.Q. Yang, "*In situ*/*operando* synchrotron-based X-ray techniques for lithium-ion battery research" *NPG Asia Materials* **10**, 563 (2018) [doi: 10.1038/s41427-018-0056-z]

123. P. Pietsch, V. Wood, "X-Ray Tomography for Lithium Ion Battery Research: A Practical Guide" *Ann. Rev. Mater. Res.* **47**, 451 (2017) [doi: 10.1146/annurev-matsci-070616-123957]

124. T. Foroozan, S. Sharifi-Asl, R. Shahbazian-Yassar, "Mechanistic understanding of Li dendrites growth by *in situ*/*operando* imaging techniques" *J. Power Sources* **461**, 228135 (2020) [doi: 10.1016/j.jpowsour.2020.228135]

125. P.P.R.M.L. Harks, F.M. Mulder, P.H.L. Notten, "*In situ* methods for Li-ion battery research: a review of recent developments" *J. Power Sources* **288**, 92 (2015) [doi: 10.1016/j.jpowsour.2015.04.084]

126. F. Lin, Y. Liu, X. Yu, L. Cheng, A. Singer, O.G. Shpyrko, H.L. Xin, N. Tamura, C. Tian, T.C. Weng, X.Q. Yang, Y.S. Meng, D. Nordlund, W. Yang, M.M. Doeff, "Synchrotron X-ray Analytical Techniques for Studying Materials Electrochemistry in Rechargeable Batteries" *Chem. Rev.* **117**(21), 13123 [doi: 10.1021/acs.chemrev.7b00007]

127. H. Liu, P.K. Allan, O.J. Borkiewicz, C. Kurtz, C.P. Grey, K.W. Chapman, P.J. Chupas, "A radially accessible tubular *in situ* X-ray cell for spatially resolved *operando* scattering and spectroscopic studies of electrochemical energy storage devices" *J. Appl. Crystal.* **49**, 1665 (2016) [doi: 10.1107/S1600576716012632]

128. Z. Deng, X. Lin, Z. Huang, J. Meng, Y. Zhong, G. Ma, Y. Zhou, Y. Shen, H. Ding, Y. Huang "Recent Progress on Advanced Imaging Techniques for Lithium-Ion Batteries" *Adv. Energy Mater.* **11**(2), 2000806 (2021) [doi: 10.1002/aenm.202000806]

129. A. Jana, R.E. Garcia, "Lithium dendrite growth mechanisms in liquid electrolytes" *Nano Energy* **41**, 552 (2017) [doi: 10.1016/j.nanoen.2017.08.056]

130. K.J. Harry, D.T. Hallinan, D.Y. Parkinson, A.A. MacDowell, N.P. Balsara, "Detection of subsurface structures underneath dendrites formed on cycled lithium metal electrodes" *Nature Materials* 13, **69** (2014) [doi: 10.1038/nmat3793]

131. J.H. Cheng, A.A. Assegie, C.J. Huang, M.H. Lin, A.M. Tripathi, C.C. Wang, M.T. Tang, Y.F. Song, W.N. Su, B.J. Hwang, "Visualization of Lithium Plating and Stripping via in *Operando* Transmission X-ray Microscopy" *J. Phys. Chem. C* **121**(14), 7761 (2017) [doi: 10.1021/acs.jpcc.7b01414]

132. S.H. Yu, X. Huang, J.D. Brock, H.D. Abruña, "Regulating Key Variables and Visualizing Lithium Dendrite Growth: An *Operando* X-ray Study" *J. Am. Chem. Soc.* **141**(21), 8441 (2019) [doi: 10.1021/jacs.8b13297]

133. S. Frisco, D.X. Liu, A. Kumar, J.F. Whitacre, C.T. Love, K.E. Swyder-Lyons, S. Litster, "Internal Morphologies of Cycled Li-Metal Electrodes Investigated by Nano-Scale Resolution X-ray Computed Tomography" *ACS Appl. Mater. Interfaces* **9**(22), 18748 (2018) [doi: 10.1021/acsami.7b03003]

134. M. Rashid, A. Gupta, "Mathematical Model for Combined Effect of SEI Formation and Gas Evolution in Li-Ion Batteries" *ECS Electrochem. Lett.* **3**(10), A95 (2014) [doi: 10.1149/2.0041410eel]

135. B. Rowden, N. Garcia-Araez, "A review of gas evolution in lithium ion batteries" *Energy Reports* **6**, 10 (2020) [doi:10.1016/j.egyr.2020.02.022]

136. F. Sun, H. Markötter, I. Manke, A. Hilger, N. Kardjilov, J. Banhart, "Three-Dimensional Visualization of Gas Evolution and Channel Formation inside a Lithium-Ion Battery" *ACS Appl. Mater. Interfaces* **8**(11), 7156 (2016) [doi: 10.1021/acsami.6b00708]

137. J. Gelb, D.P. Finegan, D.J.L. Brett, P.R. Shearing "Multi-scale 3D investigations of a commercial 18650 Li-ion battery" *J. Power Sources* **357**, 77 (2017) [doi: 10.1016/j.jpowsour.2017.04.102]

138. H. Liu, M. Wolf, K. Karki, Y.S. Yu, E.A. Stach, J. Cabana, K.W. Chapman, P.J. Chupas "Intergranular Cracking as a Major Cause of Long-Term Capacity Fading of Layered Cathodes" *Nano Lett.* **17**(6), 3452 (2017) [doi: 10.1021/acs.nanolett.7b00379]

139. *GeoDict* application from MathMarket Gmbh, available online at https://www.geodict.com/ [last verified access on 14th August 2021]

140. C.F. Holder, R.E. Schaak, "Tutorial on Powder X-ray Diffraction for Characterizing Nanoscale Materials" *ACS Nano* **13**(7), 7359 (2019) [doi: 10.1021/acsnano.9b05157]

141. K.P.C. Yao, J. S. Okasinski, K. Kalaga, I.A. Shkrob, D.P. Abraham "Quantifying lithium concentration gradients in the graphite electrode of Li-ion cells using *operando* energy dispersive X-ray diffraction" *Energy Environ. Sci.* **12**, 656 (2019) [doi: 10.1039/C8EE02373E]

142. T.R.Tanim, P.P.Paul, V. Thampy, C. Cao, H.G. Steinrück, J. Nelson Weker, M.F. Toney, E.J. Dufek, M.C. Evans, A.N. Jansen, B.J.Polzin, A.R. Dunlop, S.E.Trask "Heterogeneous Behavior of Lithium Plating during Extreme Fast Charging" *Cell Rep. Phys. Sci.* **1**(7), 100114 (2020) [doi: 10.1016/j.xcrp.2020.100114]

143. A. Raj, I.A. Shkrob, J.S. Okasinski, M.T. Fonseca Rodrigues, A.C. Chuang, X. Huang, D.P. Abraham "Spatially-resolved lithiation dynamics from *operando* X-ray diffraction and electrochemical modeling of lithium-ion cells" *J. Power Sources* **484**, 229247 (2021) [doi: 10.1016/j.jpowsour.2020.229247]

144. K.P.C. Yao, J.S. Okasinski, K. Kalaga, J.D. Almer, D.P. Abraham "*Operando* Quantification of (De)Lithiation Behavior of Silicon–Graphite Blended Electrodes for Lithium-Ion Batteries" *Adv. Energy Mater.* **9**(8), 1803380 (2019) [doi: 10.1002/aenm.201803380]

145. D.P. Finegan, A. Vamvakeros, L. Cao, C. Tan, T.M.M. Heenan, S.R. Daemi, S.D.M. Jacques, A.M. Beale, M. Di Michiel, K. Smith, D.J.L. Brett, P.R. Shearing, C. Ban "Spatially Resolving Lithiation in Silicon−Graphite Composite Electrodes via *in situ* High-Energy X-ray Diffraction Computed Tomography" *Nano Lett.***19**(6), 3811 (2019) [doi: 10.1021/acs.nanolett.9b00955]

146. D. Liu, Z. Shadike, R. Lin, K. Qian, H. Li, K. Li, S. Wang, Q. Yu, M. Liu, S. Ganapathy, X. Qin, Q.H. Yang, M. Wagemaker, F. Kang, X.Q. Yang, B. Li, "Review of Recent Development of *In Situ*/*Operando* Characterization Techniques for Lithium Battery Research" *Adv. Mater.* **31**(28), 1806620, (2019) [doi: 10.1002/adma.201806620]

147. X. Hua, R. Robert, L.S. Du, K.M. Wiaderek, M. Leskes, K.W. Chapman, P.J. Chupas, C.P. Grey, "Comprehensive Study of the CuF2 Conversion Reaction Mechanism" *J. Phys. Chem.* **118**(28), 15169 (2014) [doi: 10.1021/jp503902z]

148. K.M. Wiaderek, O.J. Borkiewicz, E. Castillo-Martínez, R. Robert, N. Pereira, G.G. Amatucci, C.P. Grey, P.J. Chupas, K.W. Chapman, "Comprehensive Insights into the Structural and Chemical Changes in Mixed-Anion FeOF Electrodes by Using *Operando* PDF and NMR Spectroscopy" *J. Am. Chem. Soc.* **135**(10), 4070 (2013) [doi: 10.1021/ja400229v]

149. R.L. Johnston, in *Metal Nanoparticles and Nanoalloys* vol. 3, 1st ed., R. Johnston, J. Wilcoxon, Editors, p. 1, Elsevier Science, Oxford (2012) [doi: 10.1016/B978-0-08-096357-0.00006-6]

150. I.F. Cruz, C. Freire, J.P. Araújo, C. Pereira A.M. Pereira, in *Magnetic Nanostructured Materials - From Lab to Fab*, A.A. El-Gendy, J.M. Barandiaran, R.L. Hadimani, Editors, p. 59, Elsevier, Amsterdam (2018) [doi: 10.1016/B978-0-12-813904-2.00003-6]

151. J. Wang, Y.C.K. Chen-Wiegart, C. Eng, Q. Shen, J. Wang, "Visualization of anisotropic-isotropic phase transformation dynamics in battery electrode particles" *Nature Commun.* **7**, 12372 (2016) [doi: 10.1038/ncomms12372]

152. A. Ulvestad, A. Singer, J. N. Clark, H. M. Cho, J. W. Kim, R. Harder, J. Maser, Y. S. Meng, O.G. Shpyrko, "Topological defect dynamics *in operando* battery nanoparticles" *Science* **348**(6241), 1344 (2015) [doi: 10.1126/science.aaa1313]

153. T. Tomieh, H. Shimizu, T. Majima, M. Yamada, T. Kanayama, H. Kondo, M. Ono "Three-Dimensional Readout of Flash X-Ray Images of Living Sperm in Water by Atomic-Force Microscopy" *Science* **252**(5006), 691 (1991) [doi: 10.1126/science.2024121]

154. A. Gianoncelli, G. Kourousias, F. Cammisuli, D. Cassese, C. Rizzardi, O. Radillo, M. Lazzarino, L. Pascolo "Combined use of AFM and soft X-ray microscopy to reveal fibres' internalization in mesothelial cells" *Analyst* **142**, 1982 (2017) [doi: 10.1039/c6an02661c]

155. G. Zan, J. Zhang, F. Monaco, S. Gul, G. Qian, J. Li, D.J. Vine, P. Cloetens, W. Yun, P. Pianetta, Y. Liu "Understanding multi-scale battery degradation with a macro-to-nano zoom through its hierarchy" *J. Mater. Chem. A*, Advance Article (2021) [doi: 10.1039/d1ta02262h]

156. R. Moroni, M. Börner, L. Zielke, M. Schroeder, S. Nowak, M. Winter, I. Manke, R. Zengerle, S. Thiele "Multi-Scale Correlative Tomography of a Li-Ion Battery Composite Cathode" *Sci. Rep.* **6**, 30109 (2016) [doi: 10.1038/srep30109]

157. O. Furat, D.P.Finegan, D. Diercks, F. Usseglio-Viretta, K. Smith, V. Schmidt "Mapping the architecture of single lithium ion electrode particles in 3D, using electron backscatter diffraction and machine learning segmentation" **483**, 229148 (2021) [doi: 10.1016/j.jpowsour.2020.229148]

158. D. Alikin, B. Slautin, A. Abramov, D. Rosato , V. Shur, A. Tselev, A. Kholkin "Correlative Confocal Raman and Scanning Probe Microscopy in the Ionically Active Particles of $LiMn_2O_4$ Cathodes" *Materials* **12**(9), 1416 (2019) [doi: 10.3390/ma12091416]

159. J.Y. Lee, J.Y. Kim, H.I. Cho, C.H. Lee, H.S. Kim, S.U. Lee, T.J.Prosa, D.J. Larson, T.H. Yu, J.P.Ahn "Three-dimensional evaluation of compositional and structural changes in cycled $LiNi_{1/3}Co_{1/3}Mn_{1/3}O_2$ by atom probe tomography"*J. Power Sources* **379**, 160 (2018) [doi: 10.1016/j.jpowsour.2018.01.042]

160. V.P. Oleshko, T. Lam, D. Ruzmetov, P. Haney, H.J. Lezec, A.V. Davydov, S. Krylyuk, J.Cumings, A.A. Talin "Miniature all-solid-state heterostructure nanowire Li-ion batteries as a tool for engineering and structural diagnostics of nanoscale electrochemical processes" *Nanoscale* **6**, 11756 (2014) [doi: 10.1039/c4nr01666a]

161. R.F. Ziesche, T. Arlt, D.P. Finegan, T.M.M. Heenan, A. Tengattini, D. Baum, N. Kardjilov, H. Markötter, I. Manke, W. Kockelmann, D.J.L. Brett, P.R. Shearing "4D imaging of lithium-batteries using correlative neutron and X-ray tomography with a virtual unrolling technique" *Nature Commun.* **11**, 777 (2020) [doi: 10.1038/s41467-019-13943-3]

162. D.P. Finegan, E. Tudisco, M. Scheel, J.B. Robinson, O.O. Taiwo, D.S. Eastwood, P.D. Lee, M. Di Michiel, B. Bay, S.A. Hall, G. Hinds, D.J.L. Brett, P.R. Shearing "Quantifying Bulk Electrode Strain and Material Displacement within Lithium Batteries via High-Speed *Operando* Tomography and Digital Volume Correlation" *Adv. Sci.* **3**(3), 1500332 (2015) [doi: 10.1002/advs.201500332]